J. Fluid Mech. (2000), *vol.* 402, *pp.* 349–378. Printed in the United Kingdom

© 2000 Cambridge University Press

Linear and nonlinear interactions between a columnar vortex and external turbulence

By TAKESHI MIYAZAKI† AND JULIAN C. R. HUNT

Department of Applied Mathematics and Theoretical Physics, University of Cambridge, Silver Street, Cambridge, CB3 9EW, UK

(Received 5 September 1997 and in revised form 31 August 1999)

The structure of initially isotropic homogeneous turbulence interacting with a columnar vortex (with circulation Γ and radius σ), idealized both as a solid cylinder and a hollow core model is analysed using the inhomogeneous form of linear rapid distortion theory (RDT), for flows where the r.m.s. turbulence velocity u_0 is small compared with Γ/σ. The turbulent eddies with scale L are distorted by the mean velocity gradient and also, over a distance L from the surface of the vortex, by their direct impingement onto it, whether it is solid or hollow. The distortion of the azimuthal component of turbulent vorticity by the differential rotation in the mean flow around the columnar vortex causes the mean-square radial velocity away from the cylinder to increase as $(\Gamma t/2\pi r^2)^2(L_x/r)u_0^2$, when $(r-\sigma) > L_x$, but on the surface of the vortices ($(r-\sigma) < L_x$) where $\langle u_r^2 \rangle$ is reduced, $\langle u_z^2 \rangle$ increases to the same order, while the other components do not grow. Statistically, while the vorticity field remains asymmetric, the velocity field of small-scale eddies near the vortex core rapidly becomes axisymmetric, within a period of two or three revolutions of the columnar vortex. Calculation of the distortion of small-scale initially random velocity fields shows how the turbulent eddies, as they are wrapped around the columnar vortex, become like vortex rings, with similar properties to those computed by Melander & Hussain (1993) using a fully nonlinear direct numerical simulation. A mechanism is proposed for how interactions between the external turbulence and the columnar vortex can lead to non-axisymmetric vortex waves being excited on the vortex and damped fluctuations in its interior. If the columnar vortex is not significantly distorted by these linear effects, estimates are made of how nonlinear effects lead to the formation of axisymmetric turbulent vortices which move as result of their image vorticity (in addition to the self-induction velocity) at a velocity of order $u_0 t\Gamma/\sigma^2$ parallel to the vortex. Even when the circulation (γ) of the turbulent vortices is a small fraction of Γ, they can excite self-destructive displacements through resonance on a time scale σ/u_0.

1. Introduction

Interactions between intense elongated vortices and surrounding turbulent motions are often produced artificially in engineering and environmental flows, and they occur naturally in most homogeneous and sheared turbulent flows. In a mixing layer, the instability of large-scale spanwise vortices, which are formed after the roll-up of Kelvin–Helmholtz billows, leads to the production of smaller-scale streamwise braids

† Permanent address: Department of Mechanical and Control Engineering, University of Electro-Communications, Chofu, Tokyo 182-8585, Japan.

https://doi.org/10.1017/S0022112099006990 Published online by Cambridge University Press

(Hussain 1986). Sarpkaya & Suthon (1991) observed experimentally that U-shaped vortices are formed on vortex tubes impinging on a free surface. These secondary structures are supposed to play substantial role in the breakup of the primary structure and in the three-dimensionalization of the flow field.

A number of basic computational studies have been undertaken on the instability of vortices and their interactions with external turbulence. Sreedhar & Ragab (1994*a*, *b*) showed, using compressible large-eddy simulations, that a centrifugally unstable columnar vortex was soon surrounded by secondary fine structures akin to counter-rotating 'vortex rings' and that they enhanced the radial exchange of angular momentum leading to the breakdown of the columnar vortex. Risso, Corjon & Stoessel (1995) and Spalart & Wray (1996) showed, numerically, how background atmospheric turbulence can stimulate the 'Crow instability' of pairs of trailing vortices and perhaps because of this axisymmetric structures are formed around each of the trailing vortices. These studies of interactions between vortices and external turbulence may help to improve modelling and understanding of mechanisms within turbulent vortices (Saffman 1973).

Melander & Hussian's (1993) numerical study concentrated on the turbulence structure around a columnar vortex by direct numerical simulations at moderately high Reynolds number using a spectral method (128^3). They followed the time evolution of a rectilinear vortex embedded in an initially homogeneous turbulence. They adjusted the intensity of the background turbulence carefully, so that secondary fine structures could form around the columnar vortex.

They observed (i) azimuthal alignment of small-scale vorticity, (ii) merger and axisymmetrization of these vortex rings and (iii) excitation of bending waves on the columnar vortex. Although the second of these is the result of nonlinear interactions between fine-scale eddies, the others seem to result from rapid distortions of turbulent eddies by the differential rotation induced by the columnar vortex. Any turbulent eddy with a radial component of vorticity is wrapped around the columnar vortex to form a structure akin to a vortex ring (or a spiral vortex) and induces deformations of the columnar vortex. The fact that fine structures are highly polarized suggests the dominance of the linear process, too. A similar mechanism was analysed by Gilbert (1993) and Bassom & Gilbert (1998) who calculated the wrapping round of the vorticity field of the external turbulence, but they did not consider the full three-dimensional vorticity field. A. Wray's (private communication) numerical simulations of an isolated vortex in a turbulent flow show how bending can lead to destruction of the vortex after about 10 rotation times. Keller & Escudier's (1980) experiments showed how axisymmetric waves on an air-core vortex in a liquid flow can grow and break up the vortex.

Our objective in this paper is to integrate the different mechanisms involved in this complex turbulence–wave problem, using the approximation of rapid distortion theory (RDT).

RDT has been found to be able to predict statistical and instantaneous turbulence structure in many kinds of homogeneous and inhomogeneous turbulent flow fields, even when the rate of distortion is 'quite' slow on the time scale of the turbulence, whenever the leading-order effect is linear in the velocity fluctuation (see, for example, Townsend 1976; Hunt & Carruthers 1990; Cambon & Scott 1999). In our vortex problem, three ingredients are present: inhomogeneous distortions of eddies caused by the differential rotation of the columnar vortex, and their interaction with the initially non-turbulent flow within the vortex tube and inertial waves on the vortex. The problem is similar to that of analysing turbulence around a bluff body (Hunt

https://doi.org/10.1017/S0022112099006990 Published online by Cambridge University Press

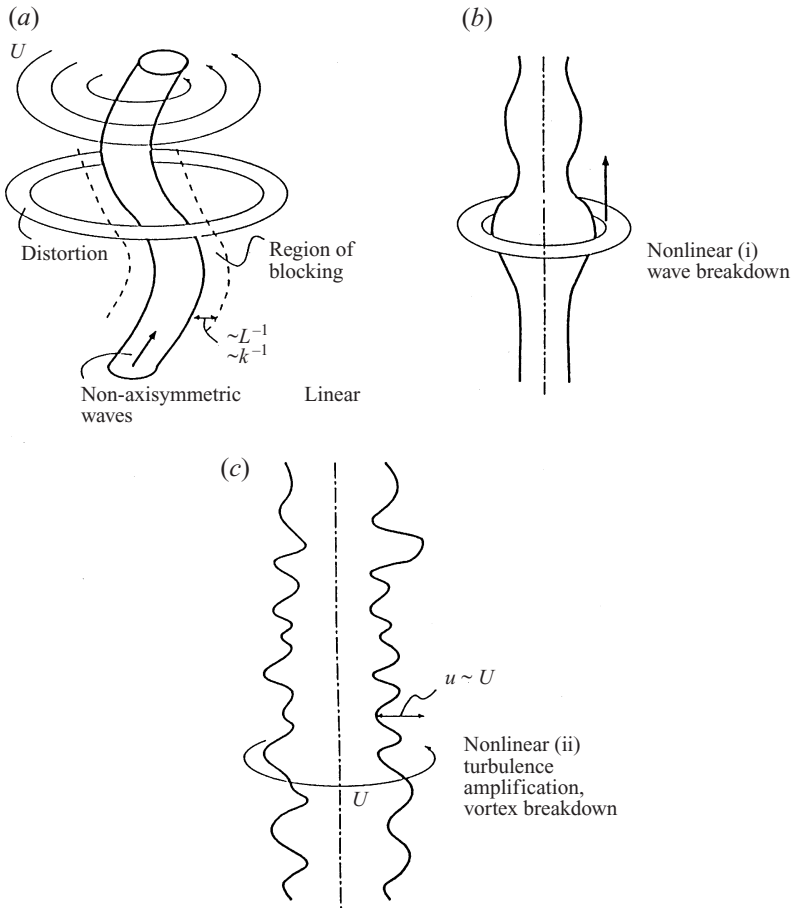


FIGURE 1. Schematic diagram of the problem. (*a*) Linear: eddy distortion and non-axisymmetric wave generation. (*b*) Nonlinear (i): excitation and breakdown of axisymmetric waves. (*c*) Nonlinear (ii): turbulence amplification and vortex breakdown.

1973), without the difficulty of the singular straining of the stagnation points, but with the extra complication of matching the external turbulence to the fluctuations generated within the vortex. This is similar to matching turbulence to waves generated in an adjacent stratified layer (Carruthers & Hunt 1986: figure 1 shows a schematic diagram).

Here we analyse the flow field at very high Reynolds number, when an external field of homogeneous isotropic turbulence interacts with three idealized types of columnar vortex.

(i) The solid cylinder model (SC) is the simplest. The core of a columnar vortex is replaced by a solid cylinder rotating with a constant angular velocity $\Omega = \Gamma/2\pi\sigma^2$. The fluid motion outside the core is irrotational with a circulation Γ. This is the simplest possible model necessary just to study the effects of differential rotation and the blocking effect of the cylinder, and is similar to sheared turbulence near a rigid wall (Lee & Hunt 1989).

(ii) Secondly, we consider a hollow core model (HC) to study the simplest kind of vortex wave excitation on the vortex. Note that this vortex is stable to any infinitesimal disturbances. Furthermore, it has only two modes if the axial and

https://doi.org/10.1017/S0022112099006990 Published online by Cambridge University Press

azimuthal wavenumbers (k_z, m) are fixed, which should be contrasted with the fact that a vortex with continuous radial vorticity distribution (including a top-hat distribution for Rankine's combined vortex) is associated with a countably infinite number of neutrally stable modes. This case provides clear understanding of the mechanisms of vortex wave generation by the distorted external turbulence.

(iii) In order to study the interactions between the turbulence and waves in the core of the vortex (which are not included in the previous cases), we also consider a third interaction where the vortex has the same density as that of the surrounding fluid and with a constant rotation vorticity in the core (solidly rotating core), i.e. Rankine's combined vortex (RCV). Although the essential mechanisms of vortex wave excitation are similar to that in case (ii), the wave-velocity field is much more complicated in and near the core of Rankine's combined vortex.

We formulate RDT for the SC model in § 2 and describe the results in § 3, where the difference between the vorticity statistics and the velocity statistics is stressed. The vortex-wave excitation is analysed using linear (RDT) theory for the HC (§ 4) and RCV models (§ 5). In § 6 we develop an order of magnitude arguments for nonlinear effects involving the generation of resonant axisymmetric waves. In the last section, the results are summarized and discussed in terms of recent computations and experiments.

2. RDT formulation for SC

We analyse the interaction between the steady irrotational flow $\boldsymbol{U}(\boldsymbol{x})$ around a columnar vortex of radius σ and circulation Γ, and an initially homogeneous turbulent velocity field $\boldsymbol{u}(\boldsymbol{x}, t)$ whose initial state at $t = 0$ is defined as $\boldsymbol{u} = \boldsymbol{u}^I(\boldsymbol{x}_0)$. We assume that the characteristic magnitude of the initial turbulent velocity field u_0, defined by the r.m.s value of the initial turbulent velocity field near the vortex so that $u_0 = \langle(\boldsymbol{u}^I)^2\rangle^{1/2}(r = \sigma)$, is much smaller than that of the vortex, i.e. $u_0 \ll \Gamma/\sigma$. The turbulent velocity field begins to be distorted by the gradients of $\boldsymbol{U}(\boldsymbol{x})$; as defined in Hunt & Carruthers (1990), this is a case of rapidly changing turbulence (RCT). It is also assumed that the Reynolds number (based on the integral scale L_x) is very large, so that the viscous effects on the energy-containing eddies are negligible. The rate of distortion of the turbulence is determined by the inhomogeneous and anisotropic strain rate of the main flow, whose magnitude is Γ/r^2, and which produces substantial geometrical distortion in the time taken for one revolution, i.e. r^2/Γ. The use of linear rapid distortion theory is justifiable for calculating the statistics of the turbulent velocity field if this time scale is small compared to the time scale on which the energy-containing eddies change as a result of nonlinear interactions between the vortices of this scale, i.e. $r^2/\Gamma \ll L_x/u_0$. This condition can be relaxed if the distortion reduces the nonlinear terms, as it does in this case (Kevlahan & Hunt 1997).

In this RDT problem the circular geometry of the distortion introduces a new aspect to the analysis, so that even if a turbulent eddy is small initially compared with length scale of the mean flow (i.e. $L_x \ll \sigma$), in the later stage of the eddy distortions it is stretched azimuthally so that it encircles the vortex, i.e. its length in one direction is comparable with that of the mean flow field. This makes the following analysis slightly more complicated than that of other RDT problems, where initially small eddies are assumed to remain small.

The essential choice in the method of RDT for analysing an inhomogeneous irrotational velocity field is between the cumbersome vorticity–streamfunction–velocity

https://doi.org/10.1017/S0022112099006990 Published online by Cambridge University Press

potential method of Hunt (1973) and the more elegant and economical velocity method developed by Goldstein (1978). We choose the latter.

The turbulent flow field at subsequent time is separated into rotational and irrotational components, as

$$\boldsymbol{u} = \boldsymbol{u}^R + \nabla\phi, \tag{1a}$$

where

$$u_i^R(\boldsymbol{x}, t) = \frac{\partial x_{0j}}{\partial x_i} u_j^I(\boldsymbol{x}_0), \tag{1b}$$

$$\Delta\phi = \nabla \cdot v\boldsymbol{u}^R. \tag{1c}$$

Here the rotational component $\boldsymbol{u}^R$ at $(\boldsymbol{x}, t)$ is directly related to the velocity $\boldsymbol{u}_j^I(\boldsymbol{x}_0)$ of the same fluid element located at x_0 at the initial time $t = 0$, in terms of the inverse of the material deformation tensor, which in RDT is determined by the velocity field $\boldsymbol{U}(x)$. Thus for given $(\boldsymbol{x}, t)$, $\boldsymbol{x}_0$ is a function of time. Since, in general, the rotational velocity field is not solenoidal, the irrotational component (with a corresponding velocity potential ϕ in (1*a*)) is introduced so as to make the whole velocity field divergence-free and to ensure that the boundary conditions are satisfied. The solution for $\boldsymbol{u}^R$ is the same for all three problems considered here. The initial and boundary conditions on $\boldsymbol{u}^R$ are

$$\boldsymbol{u}^R(\boldsymbol{x}, t) = \boldsymbol{u}^I(\boldsymbol{x}) \quad \text{at } t = 0 \tag{1d}$$

and

$$\boldsymbol{u}^R(\boldsymbol{x}, t) \to \boldsymbol{u}^I(\boldsymbol{x}) \quad \text{as } r/\sigma \to \infty, \tag{1e}$$

for $0 < t < \infty$. The above relations (1*a*, *b*, *c*), originally due to Weber (1868), have a straightforward physical derivations based on Kelvin's theorem – in terms of the partial contribution ($\int \boldsymbol{u} \cdot \mathrm{d}\boldsymbol{r}$) by fluid elements to the circulation ($\oint \boldsymbol{u} \cdot \mathrm{d}\boldsymbol{r}$) around closed loops in the flow (Hunt & Hussain 1991).

Cylindrical coordinates (r, θ, z) are convenient for representing the geometry of the problem. The z-axis coincides with the vortex axis. In order to use (1*b*), we first derive, in these coordinates, the position of a fluid element $\boldsymbol{x}$ at time t in relation to its initial position $\boldsymbol{x}_0$, using the fact that $\boldsymbol{U}(\boldsymbol{x}) = H(r - \sigma)(\Gamma/2\pi r)\boldsymbol{e}_\theta$, where $H(r - \sigma)$ is the Heaviside step function. Thence,

$$r_0 = r, \quad \theta_0 = \theta - \frac{\Gamma t}{2\pi r^2}, \quad z_0 = z. \tag{2a, b, c}$$

Here Γ denotes the circulation of the columnar vortex. The components of the rotational velocity $\boldsymbol{u}^R$ and the vorticity $\boldsymbol{\omega}^R = \nabla \wedge \boldsymbol{u} = \nabla \wedge \boldsymbol{u}^R$ are calculated to be

$$\begin{pmatrix} u_r^R \\ u_\theta^R \\ u_z^R \end{pmatrix}(\boldsymbol{x}, t) = \begin{pmatrix} 1 & \dfrac{\Gamma t}{\pi r^2} & 0 \\ 0 & 1 & 0 \\ 0 & 0 & 1 \end{pmatrix} \begin{pmatrix} u_r^I \\ u_\theta^I \\ u_z^I \end{pmatrix}, \tag{3}$$

and

$$\begin{pmatrix} \omega_r^R \\ \omega_\theta^R \\ \omega_z^R \end{pmatrix}(\boldsymbol{x}, t) = \begin{pmatrix} 1 & 0 & 0 \\ -\dfrac{\Gamma t}{\pi r^2} & 1 & 0 \\ 0 & 0 & 1 \end{pmatrix} \begin{pmatrix} \omega_r^I \\ \omega_\theta^I \\ \omega_z^I \end{pmatrix}. \tag{4}$$

https://doi.org/10.1017/S0022112099006990 Published online by Cambridge University Press

The vorticity could have been derived directly from the linearized vorticity equation (e.g. as in Hunt 1973), using the material deformation tensor.

Relation (4) shows that the θ-component of vorticity grows in proportion to time, for any general turbulent velocity field whose vorticity (at $t = 0$) has non-zero radial component. It represents the vortex stretching (and the wrapping of a vortex filament) by the differential rotation, which is the essential physical process that takes place near the columnar vortex and is discussed in detail in the following. It should be noted that Fukumoto & Miyazaki (1996) have previously identified the same physical mechanism whereby vorticity in general grows algebraically along any closed streamlines (whether circular or not) in a general potential flow field.

3. RDT-calculation for the solid cylinder vortex (SC)

3.1. *General solution*

We have to solve the Poisson equation (1c) to determine the velocity potential and thence from (1a, b) the whole velocity field:

$$\Delta\phi = -\nabla\cdot\boldsymbol{u}^R, \tag{5a}$$

$$\nabla\cdot\boldsymbol{u}^R = \frac{\Gamma t}{\pi r^2}\left[\frac{1}{r}\frac{\partial u_r^I}{\partial\theta_0} + \frac{\partial u_\theta^I}{\partial r_0} - \frac{u_\theta^I}{r} + \frac{\Gamma t}{\pi r^3}\frac{\partial u_\theta^I}{\partial\theta_0}\right]. \tag{5b}$$

Note that the relations (2a, b, c) have been used in deriving (5b). Fourier series and transforms can be defined to represent variations in the azimuthal θ- and the axial z-coordinates, because of homogeneity in these directions. The Fourier coefficients, denoted with a tilde, are defined by the integrals

$$\tilde{\phi}(r,t;k_z,m) = \frac{1}{(2\pi)^2}\int_{-\infty}^{\infty}\mathrm{d}z\int_0^{2\pi}\mathrm{d}\theta\phi(r,\theta,z,t)\,\mathrm{e}^{-\mathrm{i}(k_z z+m\theta)} \tag{6}$$

etc. Here, m and k_z denote the azimuthal and axial wavenumbers, respectively. The Poisson equation (1c) for $\tilde{\phi}$ in terms of $\tilde{u}_i$, becomes

$$\left[\frac{\partial^2}{\partial r^2} + \frac{1}{r}\frac{\partial}{\partial r} - \frac{m^2}{r^2} - k_z^2\right]\tilde{\phi} = -\left[\left(\frac{\partial}{\partial r} + \frac{1}{r}\right)\tilde{u}_r + \mathrm{i}m\tilde{u}_\theta + \mathrm{i}k_z\tilde{u}_z\right] \tag{7a}$$

$$= -\frac{\Gamma t}{\pi r^2}\exp\left(-\frac{\mathrm{i}m\Gamma t}{2\pi r^2}\right)\left[\frac{\mathrm{i}m}{r}\tilde{u}_r^I + \left(\frac{\partial}{\partial r} - \frac{1}{r} + \frac{\mathrm{i}m\Gamma t}{\pi r^3}\right)\tilde{u}_\theta^I\right], \tag{7b}$$

after substituting (5) and (6) into (7a).

Two boundary conditions are needed to solve (7). It follows from (1e) that

$$\boldsymbol{u} = \nabla\phi \to 0 \quad \text{as } \frac{r}{\sigma} \to \infty. \tag{8a}$$

The condition at the vortex core surface depends on the vortex model we are considering. For the first case of a solid cylinder at the centre of the vortex, the normal velocity of the fluctuations vanishes at the core surface, i.e.

$$\frac{\partial\tilde{\phi}}{\partial r} + \tilde{u}_r^R = 0 \quad \text{at } r = \sigma. \tag{8b}$$

Other conditions are used in §§4 and 5, when the vortex core is a fluid and its envelope fluctuates in response to pressure fluctuations caused by the turbulence.

The main result of the linear theory calculation is the linear matrix operator M_{ij}^{SC}

https://doi.org/10.1017/S0022112099006990 Published online by Cambridge University Press

that relates the Fourier coefficients of the velocity field at time t to those of initial velocity field $\boldsymbol{u}^I$, i.e.

$$\begin{pmatrix} \tilde{u}_r \\ \tilde{u}_\theta \\ \tilde{u}_z \end{pmatrix}(r,t;k_z,m) = \int_\sigma^\infty M_{ij}^{SC}(r,r',t;k_z,m) \begin{pmatrix} \tilde{u}_r^I \\ \tilde{u}_\theta^I \\ \tilde{u}_z^I \end{pmatrix}(r';k_z,m)\,\mathrm{d}r'. \tag{9}$$

The velocity field $\tilde{u}_i$ and thence the transfer matrix is given by adding the rotational $\boldsymbol{u}^R$ and irrotational components $\nabla\phi$, derived from (3) and (10a,b,c) below respectively. The contribution to the velocity potential from each initial velocity component $\tilde{u}_j^I$, for the SC case is

$$\tilde{\phi} = \tilde{\phi}_{SC} = A^{SC}(r,t)I_{|m|}(|k_z|r) + B^{SC}(r,t)K_{|m|}(|k_z|r), \tag{10a}$$

$$A^{SC}(r,t) = -\int_r^\infty r'K_{|m|}(|k_z|r')\mathrm{RHS}\,\mathrm{d}r', \tag{10b}$$

$$B^{SC}(r,t) = -\frac{\tilde{u}_r^R(\sigma)}{|k_z|K'_{|m|}(|k_z|\sigma)} + \frac{I'_{|m|}(|K_z|\sigma)}{K'_{|m|}(|k_z|\sigma)}\int_\sigma^\infty r'K_{|m|}(|k_z|r')\mathrm{RHS}\,\mathrm{d}r' - \int_\sigma^r r'I_{|m|}(|k_z|r')\mathrm{RHS}\,\mathrm{d}r'. \tag{10c}$$

Here RHS denotes the contribution to the inhomogeneous terms on the right-hand side of the Poisson equation (7). Note that ϕ and therefore the transfer operator include terms involving an integration in the radial direction. It will be shown later how this integration is involved in the calculation of the velocity statistics.

Detailed results are given in the Appendix. However, two general points need to be noted. First, expression (9) involves r'-integration, as mentioned earlier. Secondly, the radial velocity vanishes at the core surface as was required by (8b). This can be checked by putting $r = \sigma$ in (A 1a).

It is interesting to note how the mean motion of the vortex would distort a perturbation velocity field that is parallel to the vortex. If the initial velocity is a weak non-axisymmetric jet in the z-direction, and centred at (r_j,θ_j), e.g. $\boldsymbol{u}^{(I)} = u_z^{(I)}(r,\theta)\,\boldsymbol{e}_z$, $u_z^{(I)}(r,\theta) = u_j \exp[-\{(r-r_j)^2 + r_j^2(\theta-\theta_j)^2\}/l_j^2]$, the mean motion distorts the jet flow by displacing the profile through an angle $\Gamma t/2\pi r^2$ at each radius. The peak velocity is not changed, so that

$$u_z(r,\theta,t) = u_j \exp\left[-\left\{(r-r_j)^2 + r_j^2\left(\theta-\theta_j-\frac{\Gamma t}{2\pi r^2}\right)^2\right\}/l_j^2\right].$$

In the subsequent analysis, variables are non-dimensionalized on the scales of the mean flow, namely the maximum velocity $\Gamma/2\pi\sigma$ and the vortex radius σ.

3.2. *The instantaneous vorticity field*

Let us look at a typical realization of the vorticity field produced by RDT calculations, before inquiring into the statistical characteristics of the flow field, an approach first introduced by Lee, Kim & Moin (1987), who showed that these fields were similar to those obtained by full nonlinear simulations. Figure 2(a,b) illustrates the iso-vorticity surface of the initial and the later (RDT-produced) field, respectively. The initial homogeneous isotropic turbulence is produced by a direct numerical simulation of decaying turbulence, using a spectral code (512^3) (K. Yamamoto, private communication). The Reynolds number Re_λ is about 160 and we can see

https://doi.org/10.1017/S0022112099006990 Published online by Cambridge University Press

(*a*)

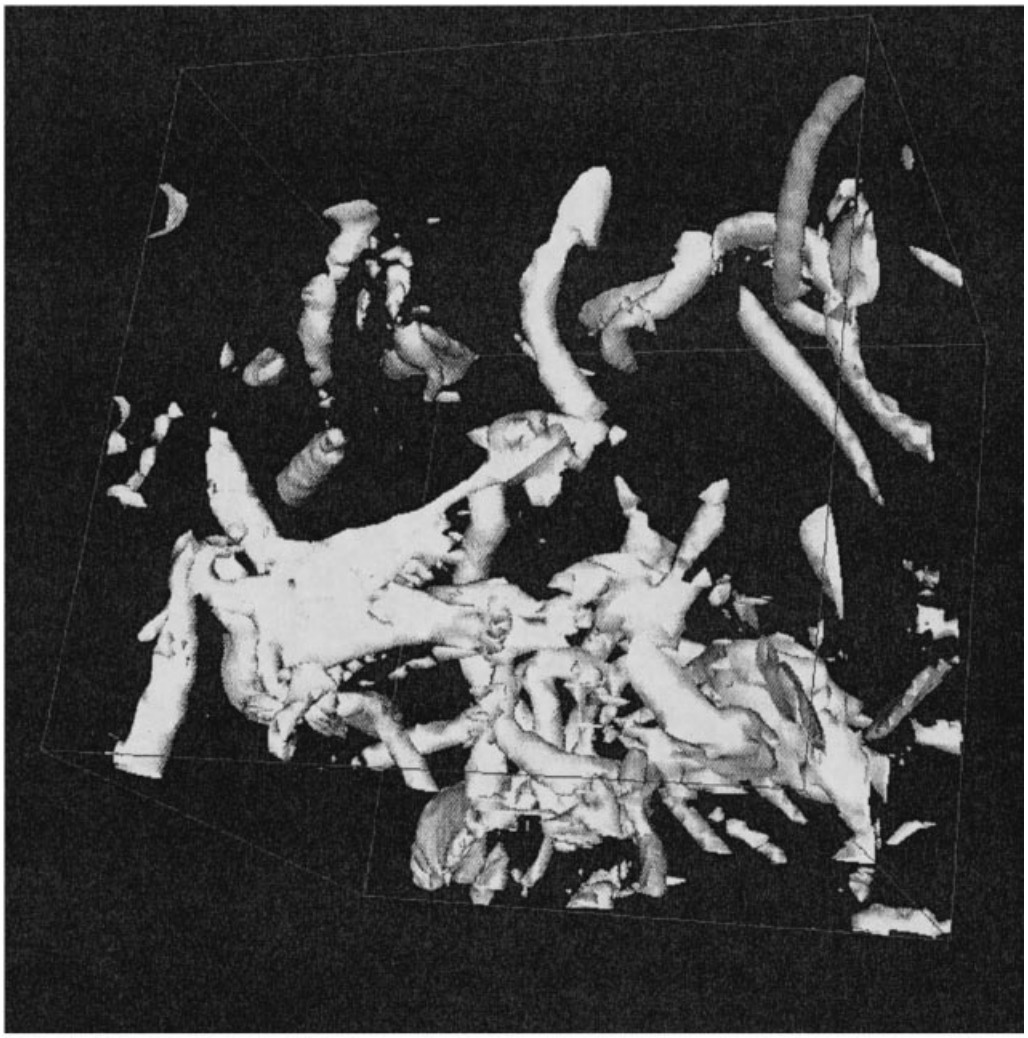


FIGURE 2 (*a*). For caption see facing page.

several intense vortices ('worms') in figure 2(*a*). Note that the normalized r.m.s. velocity is 0.82, and the integral length scale is 1.16. Thus the r.m.s. vorticity of the energy-containing eddies is 0.71. In the intense vortices the vorticity is typically 10 times the value of that in the energy-containing eddies. After a columnar vortex filament with circulation $\Gamma = \pi/2$ is introduced at the centre of the cubic flow domain (volume is π^3; the vorticity field is distorted, as shown in figure 2*b* after a half-revolution $t = \pi$ (at $r = \frac{1}{2}$). Note that the intense vortices are wrapped around the vortex filament, similar to those found in the direct numerical simulations by Melander & Hussain (1993). The vorticity of these wrapped vortices is about three times their initial value and is about 10 times the strain rate of the mean flow. This is another example of how linear RDT calculations are a good approximation for simulating the significant linear processes in distorted turbulence, in this case the

https://doi.org/10.1017/S0022112099006990 Published online by Cambridge University Press

(*b*)

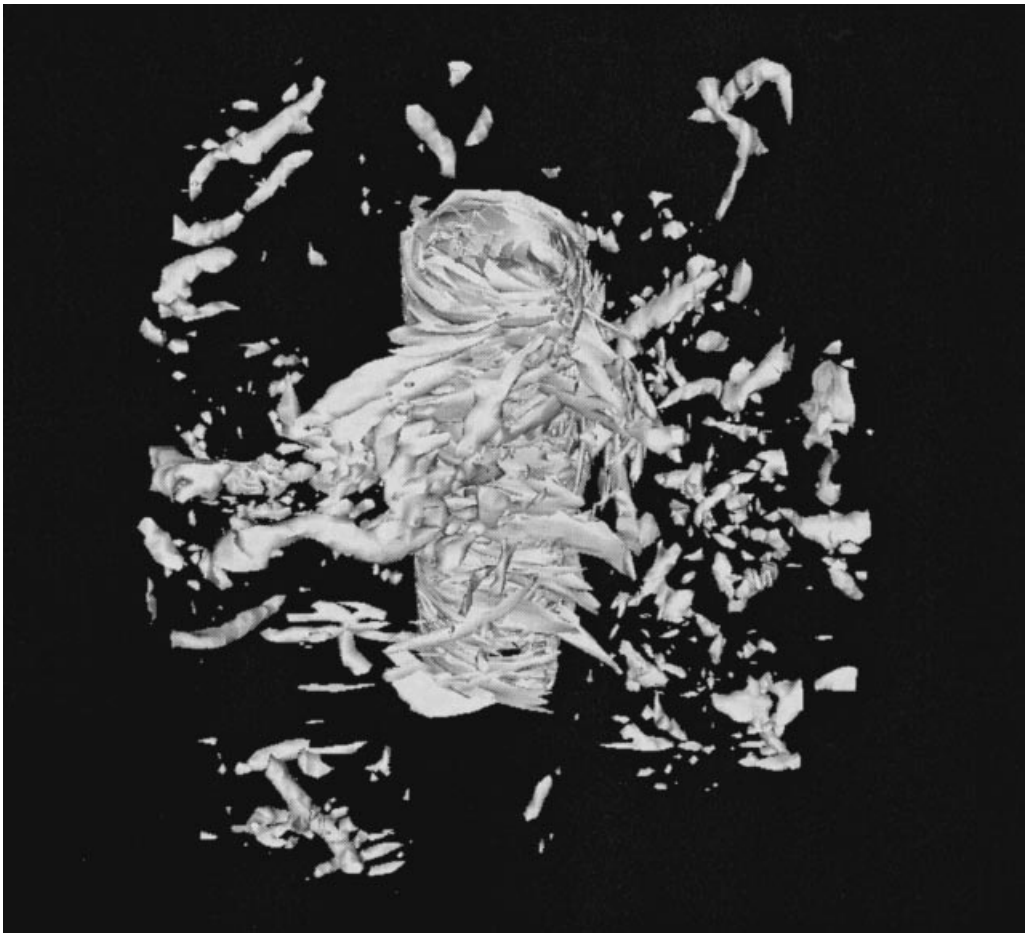


FIGURE 2. Iso-vorticity surfaces at $|\omega| = \omega_s$, in turbulence around a vortex filament of strength $\Gamma = \pi/2$ calculated by RDT: (*a*) initial state $t = 0$, $\omega_s = 8.85$ and (*b*) after half a revolution $t = \pi$, $\omega_s = 30.65$. Note that $u_0 \approx 0.8$, $L_x \approx 1.2$ so $\omega_x \approx 10u_0/L_x$ at $t = 0$.

azimuthal alignment of small-scale vorticity. The reason is that the leading nonlinear terms tend to zero in these situations (Kevlahan & Hunt 1997)).

3.3. *Vorticity statistics*

We evaluate second-order two-point correlation functions in order to study the statistical nature of the flow field near the columnar vortex. If the turbulence is statistically homogeneous in any direction, we can Fourier-decompose these functions. If, in addition it is isotropic, these particular statistics are defined by the scalar energy spectrum $E(k)$, namely

$$\Phi^I_{ij}(\boldsymbol{k}) = \frac{E(k)}{4\pi k^2}\left(\delta_{ij} - \frac{k_i k_j}{k^2}\right). \tag{11}$$

As a result of the distortion of the turbulence by the mean flow, it becomes inhomogeneous and anisotropic. However, it may remain statistically homogeneous in

https://doi.org/10.1017/S0022112099006990 Published online by Cambridge University Press

certain directions, in this case the azimuthal and axial directions. Then the correlation functions can be Fourier-decomposed in these directions, whereas the coefficients have spatial dependence on the radial coordinate, so that the two-point energy spectrum tensors $\Phi_{ij}(r_1, r_2, t; k_z, m)$ or the two-point correlations are related by

$$\langle u_i(r_1, \theta_1, z_1, t) u_j(r_2, \theta_2, z_2, t) \rangle = \sum_{m=-\infty}^{\infty} \int_{-\infty}^{\infty} \mathrm{d}k \Phi_{ij}(r_1, r_2, t; k_z, m) \exp\left[\mathrm{i}k_z(z_1 - z_2) + \mathrm{i}m(\theta_1 - \theta_2)\right]. \quad (12a)$$

Note that Φ_{ij} is related to the Fourier coefficients by the usual orthogonality relation:

$$\langle \tilde{u}_i(r_1; k_z', m') \tilde{u}_j(r_2; k_z, m) \rangle = \Phi_{ij}(r_1, r_2; k_z, m) \delta(k_z' - k_z) \delta_{mm'}. \quad (12b)$$

In order to calculate the distorted turbulence in terms of the initial homogeneous isotropic turbulence, the two-point energy spectrum tensor of the latter needs to be expressed in cylindrical coordinates and in terms of the given initial energy spectrum $E(k)$, i.e.

$$\Phi_{ij}^{I(cyl)} = \frac{1}{16\pi^2} \iiint \frac{lE(\sqrt{l^2 + k_z^2})}{(l^2 + k_z^2)^2} T_{ij} \, \mathrm{d}l \, \mathrm{d}\varphi \, \mathrm{d}\theta, \quad (13a)$$

where

$$T_{ij} = \begin{bmatrix} \alpha^c - \beta^c & \alpha^s - \beta^s & -2lk_z \cos(\varphi - \theta/2) \\ \alpha^s + \beta^s & \alpha^c + \beta^c & -2lk_z \sin(\varphi - \theta/2) \\ -2lk_z \cos(\varphi + \theta/2) & -2lk_z \sin(\varphi + \theta/2) & 2l^2 \end{bmatrix} \times \exp\left\{\mathrm{i}l[r_1 \cos(\varphi - \theta/2) - r_2 \cos(\varphi + \theta/2)] - \mathrm{i}m\theta\right\} \quad (13b)$$

and

$$\alpha^c = (l^2 + 2k_z^2)\cos\theta, \quad \alpha^s = (l^2 + 2k_z^2)\sin\theta, \quad \beta^c = l^2 \cos 2\varphi, \quad \beta^s = l^2 \sin 2\varphi. \quad (13c\text{–}f)$$

The arguments of each component of these two-point energy spectrum tensors at time t are $(r_1, r_2, t; k_z, m)$ and those for the initial 'correlation functions' are $(r_1, r_2; k_z, m)$. The above statistical representations might seem unnecessarily cumbersome but they are necessary to obtain the results derived below.

The two-point vorticity spectrum tensor Ω_{ij} can be derived in closed form, since the vorticity field (4) is given in a closed form. In dimensionless form (where the minimum mean circuit time around the columnar vortex is 2π),

$$\Omega_{ij} = \exp\left[\mathrm{i}mt\left(\frac{1}{r_2^2} - \frac{1}{r_1^2}\right)\right] Z_{ij}, \quad (14a)$$

where

$$Z_{ij} = \begin{bmatrix} \Omega_{rr}^I & -\frac{2t}{r_2^2}\Omega_{rr}^I + \Omega_{r\theta}^I & \Omega_{rz}^I \\ -\frac{2t}{r_1^2}\Omega_{rr}^I + \Omega_{\theta r}^I & \frac{4t^2}{r_1^2 r_2^2}\Omega_{rr}^I - \frac{2t}{r_1^2}\Omega_{r\theta}^I - \frac{2t}{r_2^2}\Omega_{\theta r}^I + \Omega_{\theta\theta}^I & -\frac{2t}{r_1^2}\Omega_{rz}^I + \Omega_{\theta z}^I \\ \Omega_{zr}^I & -\frac{2t}{r_2^2}\Omega_{zr}^I + \Omega_{z\theta}^I & \Omega_{zz}^I \end{bmatrix}. \quad (14b)$$

Note that $\Omega_{\theta\theta}$ grows as t^2 for any m, corresponding to the algebraic growth of

https://doi.org/10.1017/S0022112099006990 Published online by Cambridge University Press

the azimuthal vorticity component. Also, the vorticity statistics do not approach an axisymmetric state. In fact the radial variations in phase play an important role when the velocity correlation functions Φ_{ij} are evaluated. They bring about cancellation in the radial integration through rapid 'phase mixing' for large $|m|t$ for $m \neq 0$; these do not contribute to the variance which is dominated by $m = 0$.

The one-dimensional enstrophy spectrum is dominated by $\Omega_{\theta\theta}$ at large time. Summing over the angular modes m leads to a simple relation between the enstrophy k_z spectrum and the initial energy spectrum:

$$E_\Omega(r;k_z) = \sum_{m=-\infty}^{\infty} \Omega_{\theta\theta}(r,r,t;k_z,m) = \left(\frac{1}{4} + \frac{t^2}{r^4}\right) \int_{k_z}^{\infty} \left[\frac{k_z^2}{\eta} E(\eta) + E(\eta)\right] \mathrm{d}\eta. \tag{15}$$

First, this shows that the influence of the columnar vortex reaches out to a distortion radius $r_d \approx \sqrt{t}$. The azimuthal component of vorticity is built up in the region $r \leqslant r_d$ with $E_\Omega(r;k_z)$ growing in proportion to t^2 and decaying rapidly, as r^{-4}, in the radial direction. The one-dimensional enstrophy spectrum at large k_z depends on the initial energy spectrum. As with other turbulent flows distorted by irrotational velocity fields, the form of the spectrum at high wavenumber (whether an exponential or algebraic decay) is not changed by the distortion. In particular $E_\Omega(r;k_z)$ is proportional to k_z^{2-p} if the initial energy spectrum $E(\eta)$ obeys a power law η^{-p}.

3.4. *Velocity statistics*

The two-point velocity energy spectrum tensors are evaluated using the linear operator in (9) connecting the velocity field at the time t to the initial homogeneous isotropic turbulence:

$$\Phi_{ij} = \int_\sigma^\infty \mathrm{d}r_1' \int_\sigma^\infty \mathrm{d}r_2' \sum_{\alpha=1}^{3} \sum_{\beta=1}^{3} M_{i\alpha} M_{j\beta}^* \Phi_{\alpha\beta}^I. \tag{16}$$

In general these integrals with respect to the radius and therefore the energy spectra and variances cannot be expressed in closed forms. We performed the double integration numerically for an initial Gaussian energy spectrum (following Townsend 1976):

$$E(\eta) = E_0 \left(\frac{\eta}{k_0}\right)^4 \exp\left[-\left(\frac{\eta}{k_0}\right)^2\right]. \tag{17}$$

This corresponds to a distribution of typical isolated eddies as well as mean vorticity. Here, k_0 is the normalized wavenumber of the energy-containing eddies. In our calculation we take $k_0 = 5$, which implies that the turbulence length scale L_x, is about quarter of the radius of the vortex. Since the effect of 'blocking' of the radial components affects the energy-containing turbulence for a distance from the vortex of order L_x, in this case this means that the effects are only significant for $r \leqslant 1.25$. In our numerical calculation the energy level E_0 is set to 1 (thus $u_0 \approx \frac{1}{2} = (\frac{1}{3}\int_0^\infty E(\eta)\,\mathrm{d}\eta)^{1/2}$), although its value does not matter at all in the linear RDT analysis. The factor $(\eta/k_0)^4$ in front of the Gaussian, corresponding to the asymptotic form for the larger-scale eddies, enables the integration with respect to l in (13) to be carried out analytically. The other integrations in (13) are evaluated numerically using the trapezoidal summation rule with uniform discretization ($N = 200$) of the interval $[0, 2\pi]$. Similarly, the double integration with respect to the radius in (16) is evaluated

https://doi.org/10.1017/S0022112099006990 Published online by Cambridge University Press

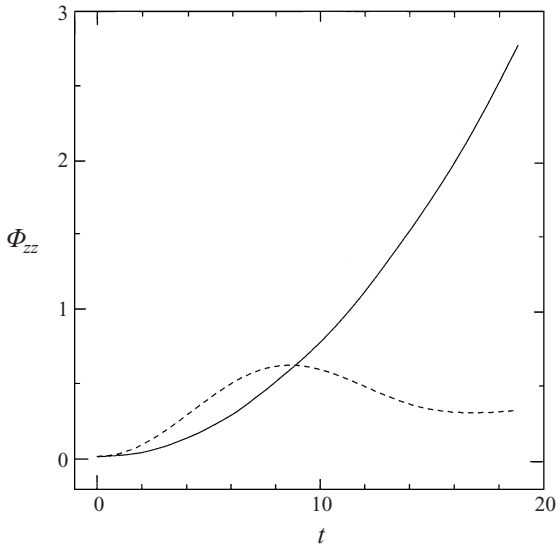


FIGURE 3. Time evolution of the spectrum function of the axial velocity: solid line, $\Phi_{zz}(1,1,t;2,0)$ (axisymmetric $m = 0$, $k_z = 2$); broken line, $\Phi_{zz}(1,1,t;4,1)$ (non-axisymmetric $m = 1$, $k_z = 4$) (normalized by the peak vortex velocity $\Gamma/2\pi\sigma^2$).

numerically using the trapezoidal summation rule with uniform discretization ($N = 200$) of the interval $[1, r_\infty = 2 + 20/|k_z|]$. The upper endpoint is selected so that the values of the integrand are less than 10^{-15} there. The radial numerical integration for large $|m|t$ becomes inaccurate because of the rapidly oscillating phase factors mentioned in the previous subsection. The following results are correct, at least, to two significant figures.

Figure 3 shows the typical time evolution of the correlation function $\Phi_{zz}(1,1,t;k_z,m)$ of axial velocity at the core surface $r = 1$. The solid line represents the axisymmetric component $m = 0$, $k_z = 2$ and the broken line denotes the asymmetric component m=1, $k_z = 4$. Both components grow as t^2, initially, at small time but only the axisymmetric one continues its growth at later time. In contrast, the growth of the asymmetric component saturates after two revolutions of the columnar vortex. This saturation results from the radial integration of a rapidly oscillating phase factor $\exp(2imt/r^2)$ as mentioned earlier. Then, quicker saturation occurs for larger $|m|$ and for smaller r. The velocity field near the core approaches a statistically axisymmetric state within two or three revolutions of the columnar vortex.

Since the numerical integration of the integrals is lengthy, it is not practical to scan a wide parameter range. Rather we concentrate on the asymptotic forms of the velocity spectra for small eddies with large $|k_z|$, and their physical interpretation. For large $|k_z|$, the contribution to the r'-integral is localized near $r' = r$, since the modified Bessel function decays exponentially. This leads to an analytic form of the integrals, with the slow variables taken as their value at $r' = r$, as in the asymptotic integrals of Hunt (1984) and Hunt & Graham (1978).

At the core surface $r = 1$, the r'-integration is performed only for $r' > r$, which yields some differences between the asymptotic forms at $r = 1$ and those at $r > 1$ and $|k_z| \to \infty$. The non-zero spectra at $r = 1$ are $\Phi_{\theta\theta}$, Φ_{zz}, $\Phi_{\theta z}$, $\Phi_{z\theta}$, and others vanish because the radial velocity vanishes at $r = 1$ on the SC. Their asymptotic forms are

https://doi.org/10.1017/S0022112099006990 Published online by Cambridge University Press

given as, for $r = 1$,

$$\Phi_{\theta\theta} = \frac{k_z^2}{k_z^2 + 4m^2t^2}\left[\frac{m^2}{k_z^2}\Phi^I_{rr} + \frac{\mathrm{i}m}{|k_z|}\Phi^I_{r\theta} - \frac{\mathrm{i}m}{|k_z|}\Phi^I_{\theta r} + \Phi^I_{\theta\theta}\right], \tag{18a}$$

$$\begin{aligned}\Phi_{zz} = {} & \frac{k_z^2}{k_z^2 + 4m^2t^2}\Phi^I_{rr} + \frac{4k_z^2t^2}{k_z^2 + 4m^2t^2}\Phi^I_{\theta\theta} + \Phi^I_{zz} + \frac{2k_z^2t}{k_z^2 + 4m^2t^2}[\Phi^I_{r\theta} + \Phi^I_{\theta r}] \\ & + \frac{\mathrm{i}k_z}{|k_z| - 2\mathrm{i}mt}\Phi^I_{rz} - \frac{\mathrm{i}k_z}{|k_z| + 2\mathrm{i}mt}\Phi^I_{zr} + \frac{2\mathrm{i}k_zt}{|k_z| - 2\mathrm{i}mt}\Phi^I_{\theta z} - \frac{2\mathrm{i}k_zt}{|k_z| + 2\mathrm{i}mt}\Phi^I_{z\theta},\end{aligned} \tag{18b}$$

$$\begin{aligned}\Phi_{\theta z} = {} & \frac{k_zm}{k_z^2 + 4m^2t^2}\Phi^I_{rr} - \frac{2\mathrm{i}k_z|k_z|t}{k_z^2 + 4m^2t^2}\Phi^I_{\theta\theta} - \frac{\mathrm{i}k_z|k_z|}{k_z^2 + 4m^2t^2}\Phi^I_{\theta r} \\ & + \frac{2k_zmt}{k_z^2 + 4m^2t^2}\Phi^I_{r\theta} + \frac{|k_z|}{|k_z| + 2\mathrm{i}mt}\Phi^I_{\theta z} + \frac{\mathrm{i}m}{|k_z| - 2\mathrm{i}mt}\Phi^I_{rz},\end{aligned} \tag{18c}$$

$$\begin{aligned}\Phi_{z\theta} = {} & \frac{k_zm}{k_z^2 + 4m^2t^2}\Phi^I_{rr} + \frac{2\mathrm{i}k_z|k_z|t}{k_z^2 + 4m^2t^2}\Phi^I_{\theta\theta} + \frac{\mathrm{i}k_z|k_z|}{k_z^2 + 4m^2t^2}\Phi^I_{r\theta} \\ & + \frac{2k_zmt}{k_z^2 + 4m^2t^2}\Phi^I_{\theta r} - \frac{|k_z|}{|k_z| - 2\mathrm{i}mt}\Phi^I_{z\theta} - \frac{\mathrm{i}m}{|k_z| + 2\mathrm{i}mt}\Phi^I_{zr}.\end{aligned} \tag{18d}$$

The argument of the initial correlation functions is $(1, 1; k_z, m)$. We can see that the terms $4m^2t^2$ and $2\mathrm{i}mt$ in the denominators bring about saturation for non-zero m. The time t_s when the saturation occurs is estimated to be $t_s \approx |k_z|/2|m|$, being smaller for smaller $|k_z|$ and for larger $|m|$. Of course, such estimates fail for 'too small' $|k_z|$, where the asymptotic forms are less accurate. As the time tends to infinity, $\Phi_{\theta\theta}$, $\Phi_{\theta z}$, $\Phi_{z\theta}$ for $m \neq 0$ decay to zero and Φ_{zz} tends to a finite limiting value, namely

$$\Phi_{zz} \approx \Phi^I_{zz}(1, 1; k_z, m) + \frac{k_z^2}{m^2}\Phi^I_{\theta\theta}(1, 1; k_z, m) - \frac{k_z}{m}[\Phi^I_{\theta z}(1, 1; k_z, m) + \Phi^I_{z\theta}(1, 1; k_z, m)]. \tag{19}$$

Actually, the above asymptotic form at large time holds for any k_z (not restricted to large $|k_z|$). Figure 4(*a*) show the axial correlation function $\Phi_{zz}(1, 1, t; k_z, 1)$ (obtained by numerical integration) as a function of $|k_z|$ at several times ($t = \pi$, 2π, 4π, 6π), with the limiting value at large time (bold solid line) from (19). We can see that the numerically integrated results (in the energy-containing range) overshoot (at $t = 2\pi$, 4π) the asymptotic value and approach it from above at large time. The axisymmetric correlation functions are

$$\Phi_{\theta\theta} = \Phi^I_{\theta\theta}(1, 1; k_z, 0) \qquad \text{(remains constant at any time)}, \tag{20a}$$

$$\Phi_{zz} \to 4t^2\Phi^I_{\theta\theta}(1, 1; k_z, 0), \tag{20b}$$

$$\Phi_{\theta z} \to -2\mathrm{i}t\,\mathrm{sgn}\,(k_z)\Phi^I_{\theta\theta}(1, 1; k_z, 0), \tag{20c}$$

$$\Phi_{z\theta} \to 2\mathrm{i}t\,\mathrm{sgn}\,(k_z)\Phi^I_{\theta\theta}(1, 1; k_z, 0). \tag{20d}$$

Note that the axisymmetric correlations, which dominate for large time, are determined by the initial azimuthal correlation function $\Phi^I_{\theta\theta}(1, 1; k_z, 0)$. We compare the numerical results in figure 4(*b*) for the axisymmetric axial correlation function $\Phi_{zz}(1, 1; k_z, 0)$ with the asymptotic estimate $t = 4\pi$, which is valid only for large $|k_z|$.

Similarly, we can evaluate the asymptotic forms for large $|k_z|$ away from the vortex

https://doi.org/10.1017/S0022112099006990 Published online by Cambridge University Press

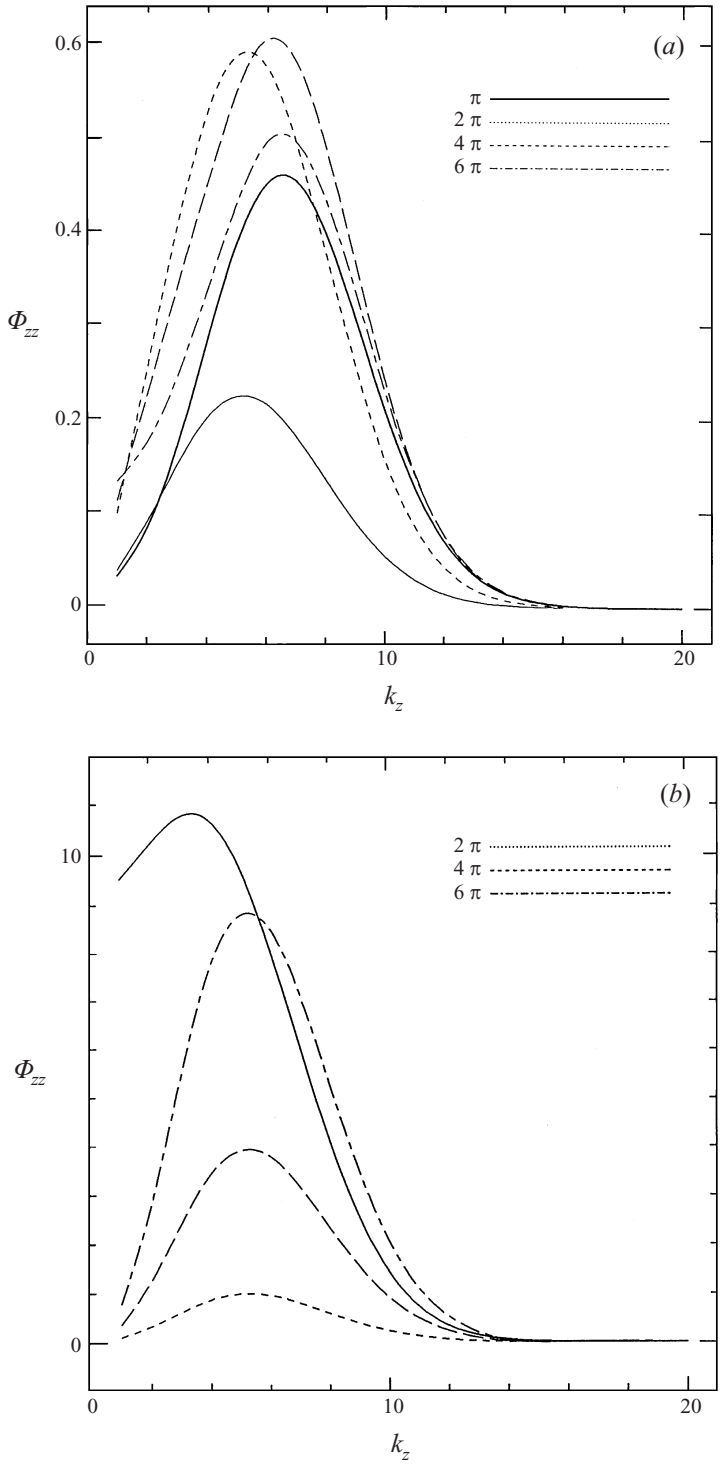


FIGURE 4. Spectrum of the axial velocity spectrum function: (*a*) non-axisymmetric $\Phi_{zz}(1,1,t;k_z,1)$ and (*b*) axisymmetric $\Phi_{zz}(1,1,t;k_z,0)$. The solid line in each figure denotes the asymptotic estimate for large $|k_z|$ (at large time in (*a*) and at $t = 4\pi$ in (*b*)).

https://doi.org/10.1017/S0022112099006990 Published online by Cambridge University Press

core surface, where $1/(r-1) \ll |k_z|$:

$$\Phi_{rr} = \frac{k_z^4}{(k_z^2 + 4m^2t^2/r^6)^2}\Phi^I_{rr} + \frac{4k_z^4t^2}{r^4(k_z^2 + 4m^2t^2/r^6)^2}\Phi^I_{\theta\theta} + \frac{2k_z^4t}{r^2(k_z^2 + 4m^2t^2/r^6)^2}[\Phi^I_{r\theta} + \Phi^I_{\theta r}], \tag{21a}$$

$$\Phi_{\theta\theta} = \frac{4m^4t^2}{r^8(k_z^2 + 4m^2t^2/r^6)^2}\Phi^I_{rr} + \frac{k_z^4}{(k_z^2 + 4m^2t^2/r^6)^2}\Phi^I_{\theta\theta} - \frac{2k_z^2m^2t}{r^4(k_z^2 + 4m^2t^2/r^6)^2}[\Phi^I_{r\theta} + \Phi^I_{\theta r}], \tag{21b}$$

$$\Phi_{zz} = \frac{4k_z^2m^2t^2}{r^6(k_z^2 + 4m^2t^2/r^6)^2}\Phi^I_{rr} + \frac{16k_z^2m^2t^4}{r^{10}(k_z^2 + 4m^2t^2/r^6)^2}\Phi^I_{\theta\theta} + \Phi^I_{zz} + \frac{8k_z^2m^2t^3}{r^8(k_z^2 + 4m^2t^2/r^6)^2}[\Phi^I_{r\theta} + \Phi^I_{\theta r}] - \frac{4k_zmt^2}{r^5(k_z^2 + 4m^2t^2/r^6)}[\Phi^I_{z\theta} + \Phi^I_{\theta z}] - \frac{2k_zmt}{r^3(k_z^2 + 4m^2t^2/r^6)}[\Phi^I_{zr} + \Phi^I_{rz}]. \tag{21c}$$

The term $4m^2t^2/r^6$ in the denominators brings about saturation for $m \neq 0$, again, when the time tends to infinity. The saturation occurs more slowly for larger r, since the saturation time t_s is factored by r^3. The terms proportional to the time t are caused by the 'initial' growth of the vorticity of disturbances in an irrotational mean strain (Batchelor & Proudman 1954). As in other distorted flows, the distortion of the wavenumbers at later time reduces the rate of growth. The only non-zero correlation function for $m \neq 0$ at large t is $\Phi_{zz}(r, r; k_z, m)$, which asymptotes to

$$\Phi^I_{zz}(r, r; k_z, m) + \frac{k_z^2r^2}{m^2}\Phi^I_{\theta\theta}(r, r; k_z, m) - \frac{k_zr}{m}[\Phi^I_{\theta z}(r, r; k_z, m) + \Phi^I_{z\theta}(r, r; k_z, m)]. \tag{22}$$

The axisymmetric correlation functions behave as

$$\Phi_{rr} \to \frac{4t^2}{r^4}\Phi^I_{\theta\theta}(r, r; k_z, 0), \tag{23a}$$

$$\Phi_{\theta\theta} = \Phi^I_{\theta\theta}(r, r; k_z, 0) \text{ (remains constant)}, \tag{23b}$$

$$\Phi_{zz} = \Phi^I_{zz}(r, r; k_z, 0) \text{ (remains constant)}. \tag{23c}$$

Note that (22) is valid for small $|k_z|$, too, and we recover the previous formula (19) at the core surface by putting $r = 1$. Away from the vortex core most of the turbulent energy is concentrated in the radial velocity component. However, at the rigid core surface this component has to be zero. The irrotational interactions caused by the rigid surface convert this blocking effect into motions parallel to the surface. Since azimuthal fluctuations (for $m = 0$) remain constant, these parallel components are in the axial direction. We illustrate the radial dependence of $\Phi_{rr}(r, r, 6\pi; 6, 0)$ and $\Phi_{zz}(r, r, 6\pi; 6, 0)$ near the core surface using numerical results in figure 5. The axial velocity dominates near the core surface but the radial velocity dominates away from the vortex core. This agrees with the results of the direct numerical simulations by Melander & Hussain (1993) and the large-eddy simulations by Sreedhar & Ragab (1994*a*, *b*).

The physical mechanism of the dominance of the radial velocity component over

https://doi.org/10.1017/S0022112099006990 Published online by Cambridge University Press

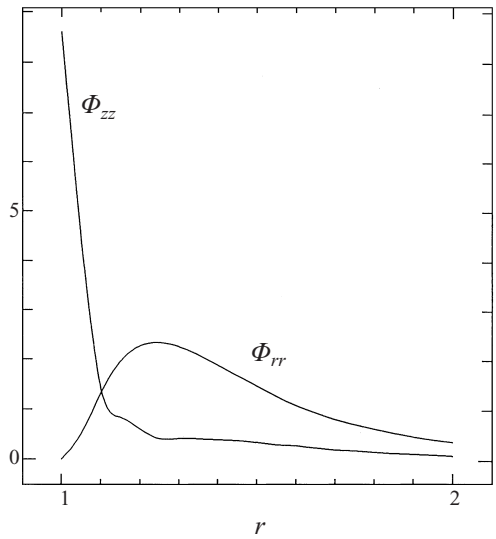


FIGURE 5. Radial dependence of the axisymmetric ($m = 0$) velocity correlation functions $\Phi_{rr}(r, r, 6\pi; 6, 0)$ (radial velocity) and $\Phi_{zz}(r, r, 6\pi; 6, 0)$ (axial velocity).

the axial velocity component is clear. The result of the distortion increases ω_θ and also reduces the length scale of radial variations, as the eddies are wrapped around the vortices like spirals. Note that as $\omega_\theta = \partial u_r/\partial z - \partial u_z/\partial r$, the relation between ω_θ and u_r is $\omega_\theta \approx \partial u_r/\partial z$. This picture is in accordance with the large-eddy simulations by Sreedhar & Ragab (1994*a*, figure 12).

As the spirals are wrapped more tightly, the linear growth of the azimuthal vorticity component tends to be saturated. However local nonlinear effects begin to be significant because the vortices are not circular but rather are disc like (Kida & Tanaka 1994). These tend to roll up from the edges near the columnar vortex and vortex rings tend to be formed. Within these motions nonlinear effects are small, but their interactions with the rigid or flexible vortices of the mean motion are nonlinear. The effect of vortex waves on the distribution of turbulence energy will be of considerable interest too, which is the subject of the next section.

Before finishing this section, we comment on the energy spectrum briefly. The one-dimensional energy spectrum

$$2E(k_z) = \sum_m (\Phi_{rr} + \Phi_{\theta\theta} + \Phi_{zz}) \tag{24}$$

is evaluated by summing over all the azimuthal modes (m). Note that the most energetic component is Φ_{zz} near the core surface and it is Φ_{rr} away from the core surface. At large time the dominant contribution comes from the axisymmetric part and the asymptotic estimate is given in terms of the initial energy spectrum tensor by the formula

$$2E(k_z) \to \frac{4t^2}{r^4}\Phi^I_{\theta\theta}(r, r; k_z, 0). \tag{25a}$$

We see that the energy grows like t^2 and that it decays rapidly in the radial direction. The decay rate is steeper than r^{-4} due to the presence of the r-dependence of $\Phi^I_{\theta\theta}(r, r; k_z, 0)$. Similarly, the spectrum decay (k_z-dependence) is slightly steeper than that of the initial homogeneous spectrum. Figure 6(*a*) shows $\Phi^I_{\theta\theta}(r, r; k_z, 0)$ as a

https://doi.org/10.1017/S0022112099006990 Published online by Cambridge University Press

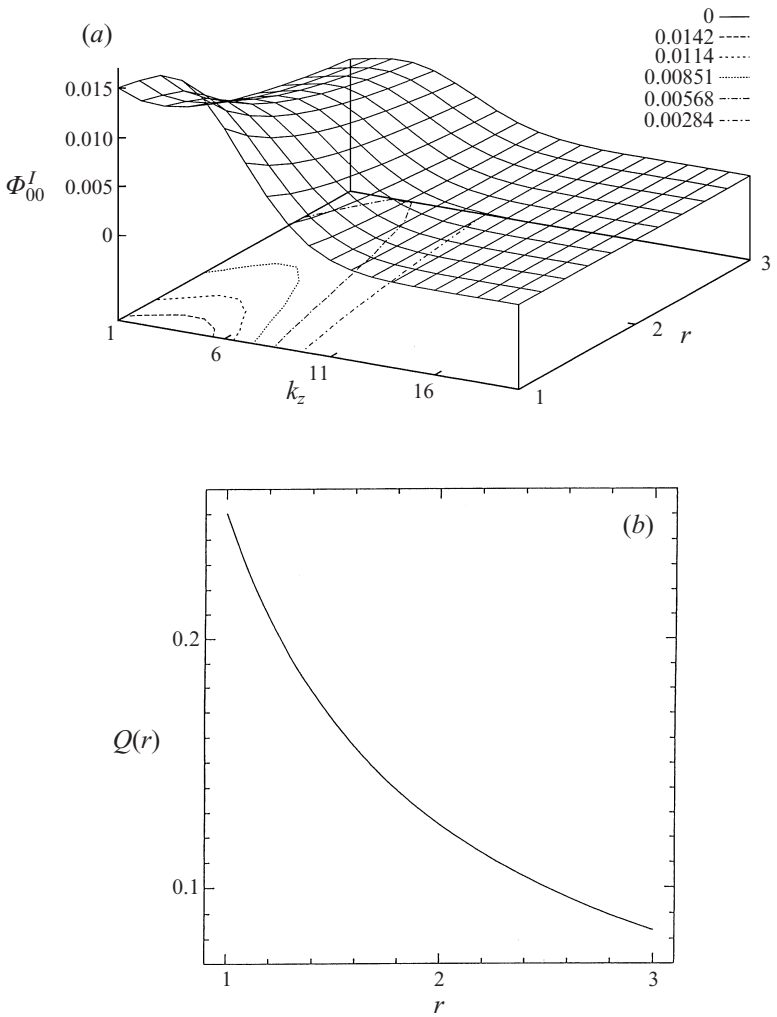


FIGURE 6. (*a*) Asymptotic one-dimensional energy spectrum $\Phi^I_{\theta\theta}(r, r; k_z, 0)$ and (*b*) asymptotic turbulence intensity $Q(r) \equiv \int_{-\infty}^{\infty} \Phi^I_{\theta\theta}(r, r; k_z, 0)\, \mathrm{d}k_z$ at large time.

function of r and k_z. It is clear that our calculated spectra do not reproduce the form of the spectrum, where $E \propto k_z^{-12}$, observed by Melander & Hussain (1993). This is inevitable because the initial spectrum was assumed to be exponential and in irrotational straining the form of the high-wavenumber spectrum is unchanged. However the errors are caused by the linear theory not modelling the nonlinear deformations of the interactions (inverse energy cascade) between azimuthally aligned vortices.

The variations in the turbulence energy can be derived by integrating (24) with respect to k_z. For large distortions (i.e. $\Gamma t/2\pi r^2 \to \infty$) the asymptotic result for the spectrum of (17) is

$$\langle |\boldsymbol{u}|^2 \rangle \to \frac{4t^2}{r^4} \int_{-\infty}^{\infty} \Phi^I_{\theta\theta}(r, r; k_z, 0)\, \mathrm{d}k_z = \frac{4t^2}{r^4} Q(r) \approx \frac{1.02t^2}{r^5}. \tag{25b}$$

The result (25*b*) can be generalized to arbitrary length scales L_x (provided L_x is small

https://doi.org/10.1017/S0022112099006990 Published online by Cambridge University Press

compared to the length of the vortex – which is assumed to be infinite); it is found that in dimensional terms for $(r-\sigma) > L_x$ or $r/L_x \gg 1$,

$$\langle u_r^2 \rangle \approx \left(\frac{\Gamma t}{2\pi r^2}\right)^2 \left(\frac{L_x}{r}\right) u_0^2. \tag{25c}$$

Note that, where surface blocking occurs, i.e. for $(r-\sigma) < L_x$ and $\sigma/L_x \gg 1$, $\langle u_r^2 \rangle$ is reduced but $\langle u_z^2 \rangle$ has about the same magnitude as $\langle u_r^2 \rangle$ away from the surface and is given by (25*c*). If the turbulence scale is much larger than that of the vortex (i.e. $L_x \gg \sigma$), the vorticity is not affected by the straining and for a Gaussian spectrum such as (17)

$$\langle u_z^2 \rangle \approx u_0^2 \left[4\left(\frac{\Gamma t}{2\pi\sigma^2}\right)^2 \left(\frac{\sigma}{L_x}\right)^2\right], \tag{25d}$$

when $r \approx \sigma$.

These asymptotic results from RDT differ from those in other flows, because here the variation with time of the turbulence energy is proportional to the energy of the vorticity. Usually $\langle |\boldsymbol{u}|^2 \rangle$ grows more slowly with time than $\langle |\omega|^2 \rangle$ because of the distortion of the wavenumbers by the strain. In this case k_r and k_z are not affected, while ω_θ increases.

Essentially (25*b*) shows that

$$u_r (\gg u_\theta, u_z) \approx \langle u_\theta (t=0) \rangle_\theta \left(\frac{\Gamma t}{2\pi r^2}\right), \tag{25e}$$

where $\langle\ \rangle_\theta$ indicates the azimuthally averaged value. For any sinusoidal function, e.g. $f = f_0 \sin\theta \exp(\mathrm{i}\boldsymbol{k}\cdot\boldsymbol{x})$, $\langle f \rangle_\theta \propto f_0/(kr)^{1/2}$ as $kr \to \infty$, and $\langle f \rangle_\theta \propto kr$ when $kr \to 0$. Thus the turbulence is determined by the initial azimuthally averaged fluctuation, and the largest velocity component is radial, except near the vortex boundary where, because of blocking, the axial velocity component is larger. The asymptotic result (25*c*) is consistent with the result in figure 6(*b*), because the variation of the function $Q(r)$ with respect to r is approximately $1/r$. For small-scale turbulence, its energy around the vortex decays like r^{-5} in the radial direction, grows like t^2 in time and increases with length scale. The result in (25*b*) is only relevant when $|k_z| \gg 1$; for larger eddies (or smaller $|k_z|$) the numerical factor 1.02 is too large, as was demonstrated in figure 4(*b*) where the asymptotic result for the axisymmetric correlation functions exceeded the numerically evaluated values for finite values of $|k_z|$.

4. Vortex-wave excitation: hollow core model

It is well known that a columnar vortex is a waveguide capable of supporting various kinds of inertial wave. Kelvin was the first who noticed this fact and he determined the dispersion relation of vortex waves on Rankine's combined vortex (Kelvin 1880). These are similar to internal gravity waves. In a stably stratified fluid (and/or surface waves at density discontinuity), the restoring force is buoyancy. Here, the centrifugal force plays the role of restoring force instead of gravity and inertial 'vortex waves' are excited. Continuous vorticity distributions correspond to continuous density stratification, for both of which there is an infinite number of modes for each set of axial and azimuthal wavenumbers.

We first consider the hollow core vortex (HC), by replacing the solid cylinder of the SC-model vortex with fluid of zero density. In this case there are only two wave

https://doi.org/10.1017/S0022112099006990 Published online by Cambridge University Press

modes (travelling upward and downward along the vortex axis) for each set of axial and azimuthal wavenumbers, just like the surface gravity waves which can propagate in the direction of the wave vector and in the opposite direction. First, we formulate the RDT problem for HC and investigate the mechanism of vortex wave generation driven by the external turbulence.

The problem for HC differs from that for SC only in one point, i.e. the boundary condition at the core surface $r = \sigma$ which is required in solving the Poisson equation (7) for the velocity potential. The condition of vanishing normal velocity (8*b*) is now replaced by the kinematic condition that the core surface moves with the fluid, and by the dynamical condition that the pressure is continuous across the interface:

$$\left(\frac{\partial}{\partial t} + \mathrm{i}m\Omega\right)\tilde{F} = \frac{\partial\tilde{\phi}}{\partial r} + \tilde{u}_r^R, \tag{26a}$$

$$\frac{\Gamma^2}{4\pi^2\sigma^3}\tilde{F} + \frac{\tilde{p}}{\rho} = 0, \quad \frac{\tilde{p}}{\rho} = \frac{\mathrm{i}}{k_z}\left(\frac{\partial}{\partial t} + \mathrm{i}m\Omega\right)(\mathrm{i}k_z\tilde{\phi} + \tilde{w}^R). \tag{26b,c}$$

Here, $\tilde{F}$ denotes the Fourier component of the surface deformation and $\Omega = \Gamma/2\pi\sigma^2$ is the angular velocity at the core surface. We arrive at the boundary condition for the potential, if we eliminate the surface deformation:

$$\left(\frac{\partial}{\partial t} + \mathrm{i}m\Omega\right)^2\left(\tilde{\phi} - \frac{\mathrm{i}}{k_z}\tilde{w}^R\right) = \Omega^2\sigma\left(\frac{\partial\tilde{\phi}}{\partial r} + \tilde{u}_r^R\right). \tag{27}$$

This condition represents a harmonic oscillator with forcing terms and indicates the excitation of surface waves on the vortex. In the absence of the forcing terms (proportional to $\tilde{u}_r^R$ and $\tilde{w}^R$), the solution for the potential that decays to zero at infinity is proportional to the modified Bessel function $K_{|m|}(|k_z|r)$ of the second kind; thence the dispersion relation for the vortex wave is obtained:

$$\left(\frac{\omega}{\Omega}\right)^2 = \frac{(\overline{\omega} - m\Omega)^2}{\Omega^2} = \frac{|k_z|\sigma K'_{|m|}(|k_z|\sigma)}{k_{|m|}(|k_z|\sigma)}. \tag{28}$$

The frequency $\overline{\omega}$ (with an overbar) is the frequency in the inertial coordinates, whereas ω denotes the frequency in the coordinates rotating around the vortex axis with the angular velocity Ω, and they are of the same order of magnitude.

The solution of the Poisson equation (7*b*) is given by adding a correction term to the potential for the SC:

$$\tilde{\phi}_{HC} = \tilde{\phi}_{SC} + \tilde{A}_{VW}(t)\frac{K_{|m|}(|k_z|r)}{K_{|m|}(|k_z|\sigma)}, \tag{29a}$$

$$\begin{aligned}\tilde{A}_{VW}(t) = \frac{1}{|k_z|\sigma K'_{|m|}(|k_z|\sigma)}\Bigg\{&\int_\sigma^\infty\left[\frac{\omega^2 t\mathrm{e}^{\mathrm{i}\omega_p t}}{\omega_p^2-\omega^2} + \frac{\mathrm{i}\omega}{2}\left(\frac{\mathrm{e}^{\mathrm{i}\omega_p t}-\mathrm{e}^{\mathrm{i}\omega t}}{(\omega-\omega_p)^2} - \frac{\mathrm{e}^{\mathrm{i}\omega_p t}-\mathrm{e}^{-\mathrm{i}\omega t}}{(\omega+\omega_p)^2}\right)\right.\\ &\left.-\frac{\sin\omega t}{\omega} + t\mathrm{e}^{\mathrm{i}\omega_p t}\right]\mathrm{e}^{-\mathrm{i}m\Omega t}\frac{\mathrm{i}m\Gamma}{\pi r'^2}K_{|m|}(|k_z|r')\tilde{u}_\theta^I(r')\,\mathrm{d}r'\\ &-\int_\sigma^\infty\left[\frac{\omega^2 t\mathrm{e}^{\mathrm{i}\omega_p t}}{\omega_p^2-\omega^2} + \frac{\mathrm{i}\omega}{2}\left(\frac{\mathrm{e}^{\mathrm{i}\omega_p t}-\mathrm{e}^{\mathrm{i}\omega t}}{(\omega-\omega_p)^2} - \frac{\mathrm{e}^{\mathrm{i}\omega_p t}-\mathrm{e}^{-\mathrm{i}\omega t}}{(\omega+\omega_p)^2}\right)\right.\\ &\left.-\frac{\sin\omega t}{\omega} + t\mathrm{e}^{\mathrm{i}\omega_p t}\right]\mathrm{e}^{-\mathrm{i}m\Omega t}\frac{|k_z|\Gamma}{\pi r'^2}K'_{|m|}(|k_z|r')\tilde{u}_\theta^I(r')\,\mathrm{d}r'\Bigg\},\end{aligned} \tag{29b}$$

https://doi.org/10.1017/S0022112099006990 Published online by Cambridge University Press

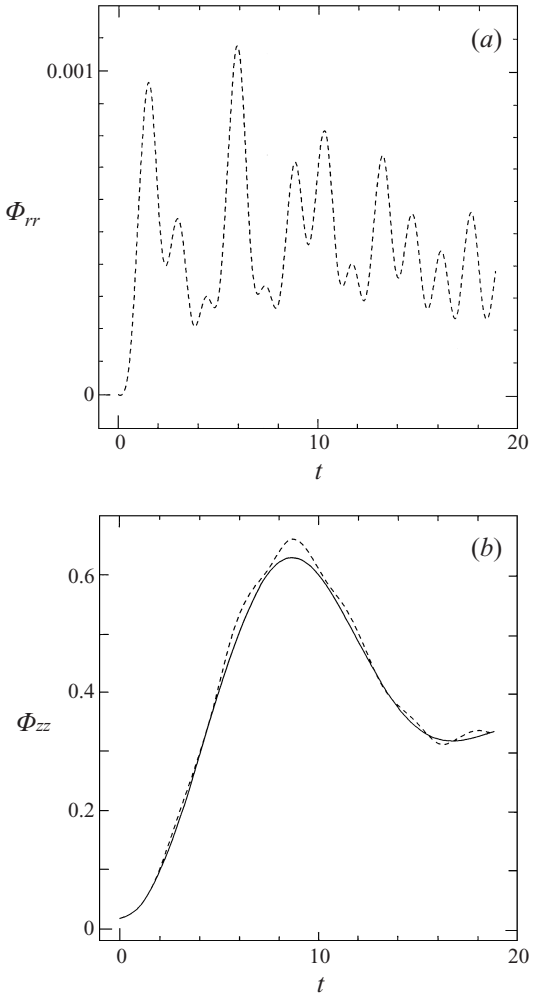


FIGURE 7. (*a*) Spectrum of radial velocity $\Phi_{rr}(1,1,t;4,1)$ and (*b*) of axial velocity $\Phi_{zz}(1,1,t;4,1)$ on the surface of the vortex for the hollow core vortex model (HC: broken lines). The solid line represents the solid cylinder model (SC).

with $\omega_p \equiv m(1-1/r'^2)$. The 'apparent' resonance at $\omega = \omega_p$ is not a real one, since the numerator vanishes there, too. These formulae are same as those of Ffowcs Williams & O'Shea (1970) in the limit of $c \to \infty$, $k \to 0$.

Two initial conditions are required to determine the amplitude coefficient $\tilde{A}_{VW}(t)$. The above solution (29*b*) is obtained when the vortex starts from a state of rest, i.e. at $t = 0$

$$\tilde{A}_{VW} = \frac{\mathrm{d}\tilde{A}_{VW}}{\mathrm{d}t} = 0. \qquad (30a,b)$$

These conditions imply that the forcing by the turbulence determines the initial core surface deformation $\tilde{F}(t=0) = \tilde{F}_0$ (cf. (26*b*,*c*)) and that any 'free' oscillations can be ignored. As in (9) the solution for HC can once again be expressed in terms of a

https://doi.org/10.1017/S0022112099006990 Published online by Cambridge University Press

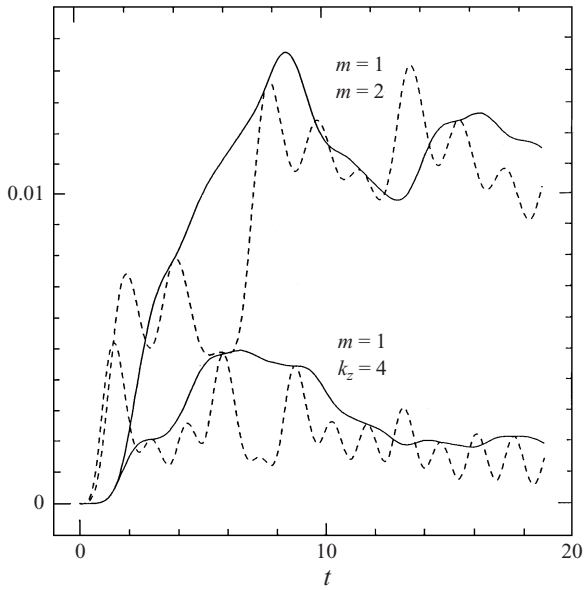


FIGURE 8. Spectra of the excess core deformation $\Phi_{\Delta F} = \langle(\tilde{F} - \tilde{F}_0)^2\rangle$ (solid lines) and the total core deformation $\Phi_F = \langle\tilde{F}^2\rangle$ (broken lines) when the initial core displacement is zero, i.e. $\tilde{F}_0 = 0$. Here the wavenumbers are $(k_z, m) = (2, 1)$ and (4,1).

modified linear operator:

$$\begin{pmatrix} \tilde{u}_r \\ \tilde{u}_\theta \\ \tilde{u}_z \end{pmatrix}(r, t; k_z, m) = \int_\sigma^\infty M_{ij}^{HC}(r, r', t; k_z, m) \begin{pmatrix} \tilde{u}_r^I \\ \tilde{u}_\theta^I \\ \tilde{u}_z^I \end{pmatrix}(r'; k_z, m)\, \mathrm{d}r'. \tag{31}$$

It is a striking result that no forced axisymmetric wave is excited by the linear interaction between the external turbulence and the hollow core, despite the fact that only the axisymmetric velocity spectra grow in time. This follows from the formula (29*b*) for $\tilde{A}_{VW}(t)$, which vanishes if we put $m = 0$ ($\omega_p = 0$). This apparent paradox is resolved later, when we examine asymmetric vortex wave generation.

Figure 7(*a*) shows the spectrum of the radial velocity at typical wavenumbers $\Phi_{rr}(1, 1, t; 4, 1)$ at the surface of the hollow core as a function of time. This component is only produced by the vortex waves, since the radial velocity is zero at $r = 1$ on the solid core vortex (SC). Note that it does not grow with time but oscillates with a small amplitude. For large $|k_z|$, the asymptotic form can be derived explicitly as

$$\Phi_{rr} = \frac{64m^2}{\omega^4}\left[\frac{k_z^2 - 2\cos\omega t(k_z^2 - 12m^2t^2)}{(k_z^2 + 4m^2t^2)^3} + \frac{\cos^2\omega t}{k_z^4}\right] \times(m^2\Phi_{rr}^I + \mathrm{i}m|k_z|\Phi_{r\theta}^I - \mathrm{i}m|k_z|\Phi_{\theta r}^I + k_z^2\Phi_{\theta\theta}^I). \tag{32}$$

At large time, it asymptotes to

$$\Phi_{rr} \to \frac{64m^4\cos^2\omega t}{\omega^4 k_z^4}\left(\Phi_{rr}^I + \frac{\mathrm{i}|k_z|}{m}\Phi_{r\theta}^I - \frac{\mathrm{i}|k_z|}{m}\Phi_{\theta r}^I + \frac{k_z^2}{m^2}\Phi_{\theta\theta}^I\right). \tag{33}$$

Thus the radial correlation remains small (of the order of its initial value). Figure 7(*b*) compares the time evolution of the spectra of the axial components for the

https://doi.org/10.1017/S0022112099006990 Published online by Cambridge University Press

hollow core vortices, namely $\Phi_{zz}^{HC}(1,1,t;4,1)$ and $\Phi_{zz}^{SC}(1,1,t;4,1)$. The difference is very small, in much the same way that the energy-containing parts of the spectra of the components of velocity parallel to a rigid surface are not much affected by it except at the smaller scales (Hunt 1984). The hollow core surface movements have almost no effect on the velocity field away from the core surface since it decays exponentially as r increases.

Figure 8 shows the time evolution of the spectra for the 'excess' deformation $\Phi_{\Delta F} = \langle(\tilde{F} - \tilde{F}_0)^2\rangle$, where $\tilde{F}_0$ denotes the initial deformation and of the deformation $\Phi_F = \langle\tilde{F}'^2\rangle$ starting from the more natural initial conditions $\tilde{A}_{VW} = \tilde{F}' = 0$. The spectra saturate to almost the same value after two or three revolutions of the columnar vortex in both cases, although the initial growth is proportional to t^4 for the solid line and to t^2 for the broken line. The asymptotic expression for large $|k_z|$ is

$$\Phi_{\Delta F} \approx \left[\frac{1}{\omega^4(k_z^2+4m^2t^2)^2} + \frac{1}{\omega^4 k_z^4} + \frac{16m^2\sin^2\omega t}{\omega^6 k_z^6} - \frac{2(k_z^2-4m^2t^2)}{\omega^4(k_z^2+4m^2t^2)^2k_z^2} - \frac{32m^2t\sin\omega t}{\omega^5(k_z^2+4m^2t^2)^2k_z^2}\right]\left(\Phi_{rr}^I + \frac{\mathrm{i}|k_z|}{m}\Phi_{r\theta}^I - \frac{\mathrm{i}|k_z|}{m}\Phi_{\theta r}^I + \frac{k_z^2}{m^2}\Phi_{\theta\theta}^I\right). \tag{34}$$

At large time this expression becomes

$$\Phi_{\Delta F} \to \frac{1}{\omega^4 k_z^4}\left(1 + \frac{16m^2\sin^2\omega t}{k_z^2}\right)\left(\Phi_{rr}^I + \frac{\mathrm{i}|k_z|}{m}\Phi_{r\theta}^I - \frac{\mathrm{i}|k_z|}{m}\Phi_{\theta r}^I + \frac{k_z^2}{m^2}\Phi_{\theta\theta}^I\right). \tag{35}$$

Thus, asymptotically, the amplitude oscillates about a constant value, which is larger for smaller $|k_z|$ and for smaller $|m|$. Although the asymptotic form is less accurate for small $|k_z|$, the results obtained by numerically evaluated integrals support this conclusion. Also, it is consistent with the direct numerical simulations by Melander & Hussain (1993). They observed long bending waves (not axisymmetric waves) on the vortex core, even though the statistics of the velocity field around the core rapidly become axisymmetric.

We note the close relation between the correlation of the surface deformation and the azimuthal velocity correlation, for their asymptotic forms have the common factor

$$\Phi_{rr}^I + \frac{\mathrm{i}|k_z|}{m}\Phi_{r\theta}^I - \frac{\mathrm{i}|k_z|}{m}\Phi_{\theta r}^I + \frac{k_z^2}{m^2}\Phi_{\theta\theta}^I. \tag{36}$$

This is not surprising because the pressure defect at linear order is proportional to the azimuthal turbulent velocity. The spectrum of the azimuthal velocity decays as time tends to infinity, which means the forcing vanishes at large time and the total energy input to vortex waves remains finite. Then the amplitude of vortex waves cannot grow without limit.

The reason why no axisymmetric vortex wave is excited in the linear approximation is given by a similar argument. The axisymmetric azimuthal velocity remains at its initial value, since the azimuthal component of the rotational velocity $\boldsymbol{u}^R(\boldsymbol{x},t)$ (3) is time-independent. Also, no axisymmetric correction comes from the potential flow component $\nabla\phi$. Then, no forced axisymmetric vortex wave is generated, because the initial pressure defect associated with the initial turbulent velocity field is balanced by the initial deformation $\tilde{F}_0$. This fact is not sensitive to the choice of the vortex model in the RDT formulation, as we see in the next section.

https://doi.org/10.1017/S0022112099006990 Published online by Cambridge University Press

5. Rankine's combined vortex

So far we have studied the vortex–turbulence interaction using RDT, for two idealized models of the vortex, one with a solid core (SC) and the other with a hollow core (HC). Although these models usefully capture the essence of the phenomena (and the hollow core model might have direct relevance to experiments such as those of Keller & Escudier 1980), they do not account for all the significant interactions between the external turbulence and the motion within a columnar fluid vortex.

The simplest realistic model of a columnar fluid vortex is Rankine's combined vortex (RCV), defined as a solidly rotating vortex core and a potential flow (with circulation Γ) surrounding the core. The RDT problem, as before, consists of calculating the change to an initially defined perturbation velocity field $\boldsymbol{u}^I(\boldsymbol{x})$. Now it is also necessary to solve the linearized Euler's equation of motion for $\boldsymbol{u}^{(c)}(\boldsymbol{x},t)$ inside the vortex core which is driven by the velocity fluctuations at $r=\sigma$. It is assumed that there are no initial rotational fluctuations in the core so that $\nabla\wedge\boldsymbol{u}^{(c)}(\boldsymbol{x},t)=0$ at $t=0$. It is known that in a uniform angular velocity a homogeneous random velocity field at linear order is simply rotated and not amplified (Cambon & Jacquin 1989), but because, in this inhomogeneous flow, they are matched to the external flow at the surface of the vortex, they are amplified as a result of amplification of the external turbulence. This leads to a growing solution for $\boldsymbol{u}^{(c)}(\boldsymbol{x},t)$ and the internal fluctuations affect the potential ϕ outside the core. It is, however, not possible to derive a simple condition (like (27) in the case of HC), since there is now an infinite number of vortex-wave modes for each set of (k_z, m). We must resort to a more systematic method, such as the Laplace transformation in time. These modes, after some straightforward (but lengthy) algebraic manipulations, are derived systematically in terms of the Laplace-transformed velocity potential:

$$\tilde{\phi}_{RCV}=\tilde{\phi}_{SC}+\tilde{A}_{RCV}(t)\frac{K_{|m|}(|k_z|r)}{K_{|m|}(|k_z|\sigma)},\quad r>\sigma, \tag{37a}$$

$$\hat{A}_{RCV}(S)=\int_0^\infty \tilde{A}_{RCV}(t)\exp(-st)\,\mathrm{d}t, \tag{37b}$$

$$\begin{aligned}\hat{A}_{RCV}(S)=&\frac{(s+\mathrm{i}m)^2[BJ'_{|m|}(\beta)/J_{|m|}(\beta)]+2\mathrm{i}m(s+\mathrm{i}m)}{\dfrac{(s+\mathrm{i}m)^2\beta J'_{|m|}(\beta)}{|k_z|K'_{|m|}(|K_z|)J_{|m|}(\beta)}+\dfrac{2\mathrm{i}m(s+\mathrm{i}m)}{|k_z|K'_{|m|}(|k_z|)}-\dfrac{(s+\mathrm{i}m)^2+4}{K_{|m|}(|k_z|)}}\\&\times\left\{\int_1^\infty\frac{2\mathrm{i}m/r'^2}{(s+\mathrm{i}m/r'^2)^2}K_{|m|}(|k_z|r')\tilde{u}_r^I(r')\,\mathrm{d}r'\right.\\&\left.-\int_1^\infty\frac{2|k_z|/r'}{(s+\mathrm{i}m/r'^2)^2}K'_{|m|}(|k_z|r')\tilde{u}_\theta^I(r')\,\mathrm{d}r'\right\}\end{aligned} \tag{37c}$$

with

$$\beta=|k_z|\sqrt{-1-\frac{4}{(s+\mathrm{i}m)^2}}.$$

As before, in our convenient normalization $\Gamma=2\pi$, $\sigma=1$. The contributions to the inverse Laplace transformation, which is an integration in the complex s-plane, come from those around the poles and those along the branch cuts of β. The integrations along the branch cuts, however, give no contribution in this case. The poles are classified into two types. The first type is the zeros of the denominator outside the r'-integrals, which corresponds to free vortex waves. Actually, there is an infinite number

https://doi.org/10.1017/S0022112099006990 Published online by Cambridge University Press

of discrete poles (Kelvin 1880). For the forced oscillations we consider here, the free vortex waves can be eliminated. Then, the double pole at $s = -\mathrm{i}m/r'^2$ indicates the possibility of large-amplitude excitation of forced waves on the Rankine vortex, as on the hollow core vortex.

However, our analysis has shown that there is no significant forcing of axisymmetric disturbances by the turbulence (i.e. $m = 0$). Therefore there can be no significant excitation of axisymmetric waves as a result of the linear distortion. Only asymmetric waves of finite amplitude are generated, as in the case of HC. The numerics in this case are more subtle because of the accidental coincidence of the double pole of the forced oscillation with some of the poles corresponding to free oscillations, since the double pole moves along the imaginary axis from $-\mathrm{i}m$ to the origin during the r'-integration. There was a similar triple pole in the numerical integration for HC; its contribution to the amplitude of the vortex wave (with $|m| \geqslant 2$) has not been determined accurately. However, its effect is small and we consider that the wave generation phenomena for RCV are qualitatively the same to those for HC.

6. Discussion of waves on the vortex

The linear RDT predicts the azimuthal alignment of the fine-scale structure of the external turbulence and the formation of randomly oriented vortex rings around the columnar vortex, but no axisymmetric pressure fluctuations. As a consequence the linear analylsis implies that no axisymmetric waves are excited. In this section we consider how, if the columnar vortices are not significantly distorted by the asymmetric linear pressure fluctuations, weakly nonlinear effects lead to axisymmetric pressure fluctuations, in order to estimate how resonances could destroy vortices. There are several steps in reaching this result, which are all found in previously published papers.

First, these intense vortex rings (even if not exactly axisymmetric) tend to travel along the vortex axis, as a result of their own induction. The sweeping action of large-scale turbulence could also add another random element to this translation as occurs at density interfaces (Carruthers & Hunt 1986). In this problem the ring velocity, itself, is proportional to u_0 and therefore is not taken into account in the linear RDT analysis. Secondly, these vortex rings may interact with each other. Melander & Hussain (1993) noted the occurrence of such interactions in their direct numerical simulations and observed how they led to vortex rings enlarging through merger and thence an inverse energy cascade to large scales. Thirdly, a second-order pressure perturbation produced by (and moving with) the turbulent vortices can excite waves on the central vortex. If the velocity of a turbulent vortex is close to the group velocity of a certain vortex wave, it must excite resonantly a large-amplitude vortex wave. Finally, this process may cease either when turbulent vortex rings break up, e.g. due to unstable asymmetric disturbances, or when axisymmetric vortex oscillaitons become large enough to destroy it. We discuss these nonlinear effects for the idealized problem of a hollow core vortex with a circular vortex ring surrounding it and conclude with an order of magnitude estimate for the breakup time. Marshall's (1997) analysis reveals many of the features of these nonlinear interactions but he does not come to our general conclusion.

The velocity C of a thin vortex ring is the sum of two components: C_S, the self-induction velocity, and C_I the velocity induced by the image of the ring in the columnar vortex, i.e.

$$C = C_S + C_I, \tag{38a}$$

https://doi.org/10.1017/S0022112099006990 Published online by Cambridge University Press

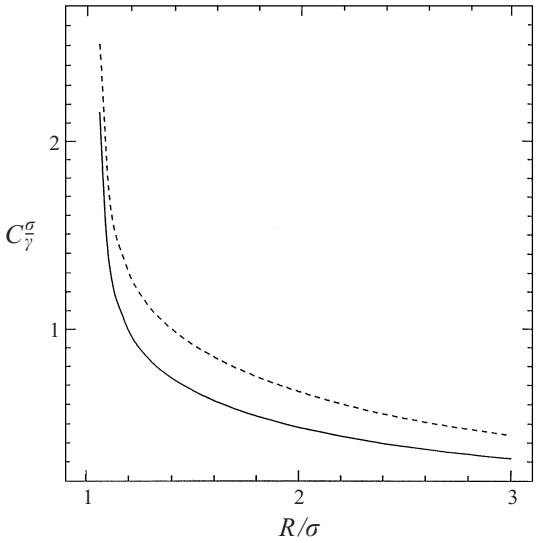


FIGURE 9. Velocity C of a vortex ring: solid line, $a/\sigma = 10^{-2}$ and broken line, $a/\sigma = 10^{-3}$.

where

$$C_S = \frac{\gamma}{4\pi R}\log\left(\frac{1+\cos\delta_\theta}{1-\cos\delta_\theta}\right), \tag{38b}$$

$$C_I = \frac{\gamma R}{\pi}\int_0^\infty \frac{kI_1(k\sigma)}{K_1(k\sigma)}K_1(kR)K_0(kR)\,\mathrm{d}k. \tag{38c}$$

Here, γ is the circulation of the vortex ring and $R\,(>\sigma)$ is the ring radius. The first term denotes the self-induction, where δ_θ is the cut-off factor. For a solidly rotating core, it is given by

$$\delta_\theta = \frac{a}{4R}\mathrm{e}^{3/4}, \tag{39}$$

with a being the assumed filament core radius (see, for example, Saffman 1992). The velocity induced by the image (38c) is calculated up to second order, assuming that the vortex ring travels parallel to (or coaxially with) a cylindrical hollow core vortex of fixed radius σ. The deformation of a hollow core surface occurs at second order and, then, the correction to the image-induced velocity appears at third order. Figure 9 shows the vortex ring velocity C as a function of the ring radius R for two values of the cut-off parameter δ_θ corresponding to $a/\sigma = 10^{-2}$, 10^{-3}. The velocity, especially that induced by the image vortex, increases rapidly as R decreases (tends to 1 from above).

The radial deformation $F(z)$ of the hollow core up to second order is obtained by evaluating the pressure defect at second order, as

$$F(z) = \frac{2\pi^2\sigma^3}{\Gamma^2}(C^2 - W^2), \tag{40a}$$

$$W = -C + \frac{\gamma R}{2}\int_0^\infty k\mathrm{e}^{-kz}J_1(kR)J_0(k\sigma)\,\mathrm{d}k + \frac{\gamma R}{\pi}\int_0^\infty \frac{kI_1(k\sigma)}{K_1(k\sigma)}K_1(kR)K_0(k\sigma)\cos kz\,\mathrm{d}k. \tag{40b}$$

https://doi.org/10.1017/S0022112099006990 Published online by Cambridge University Press

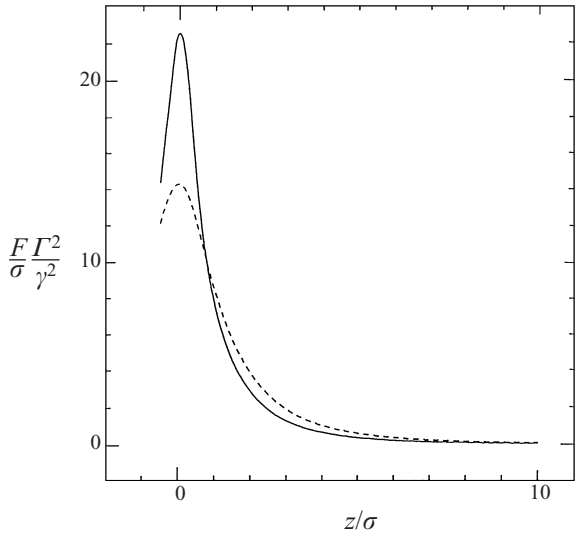


FIGURE 10. Second-order axisymmetric core deformation induced by a travelling vortex ring with circulation γ, in relation to the circulation of the vortex Γ: solid line, $R/\sigma = 2.0$ and broken line, $R/\sigma = 1.5$.

Note that the maximum value $F(0) \approx \gamma^2\sigma/\Gamma^2$. We show in figure 10, as a function of z, the vortex core deformation (expansion) induced by vortex rings of radius $R = 1.5$ and 2 with the cut-off $a/\sigma = 10^{-2}$. The striking feature of this result is that, even if the circulation of the vortex ring is about $\frac{1}{5}$ of the columnar vortex, the deformation may be as large as the core radius!

The kind of strong interaction can also be understood by comparing the pressure defect induced by the vortex ring at radius R, which is $O(\rho(\gamma/(R-\sigma))^2)$, with the pressure field $[O(\rho(\Gamma/R)^2)]$ produced by the columnar vortex. This condition is also satisfied if the group velocity $C_g = \mathrm{d}\omega/\mathrm{d}k_z \approx \Gamma/\sigma$ of the wave on the vortex is close to the propagation velocity C_γ of the vortex ring, where $C_\gamma \approx \gamma/(R-\sigma)$ for $R \geqslant (\sigma + L_x)$ with L_x being the scale of the vortex. This result indicates that smaller vortices or eddies resonate first. Note that the circulation $\gamma = \Gamma(R-\sigma)tu_0/\sigma^2$ of any induced vortex ring made up of distorted azimuthal vortex lines grows in proportion to time, although that of an exactly circular ring remains constant. Thus for eddies where $L \approx \sigma$ resonance is expected to occur after a time of $O(\sigma/u_0) \approx L/u_0$. Here we assume that the length scale L_x of the turbulence is of the order of the vortex radius σ. If L_x is much larger than σ, the pressure perturbation occurs at a larger scale and the interaction is weaker.

When the external turbulence has a larger length scale than that of the vortex (i.e. $L_x \gg \sigma$), its interaction can be estimated by considering eddies in the Kolmogorov inertial-range spectrum. Then from the above results the eddy that undergoes maximum amplification has a length scale (l) comparable with σ. Its initial energy is of order $\varepsilon^2\sigma^{2/3}$ and after the distortion it is $(\Gamma t/2\pi\sigma^2)^2\varepsilon^{2/3}\sigma^{2/3}$. Here ε is a rate of dissipation per unit mass. Now let t_{ed} be the eddy deformation time over which the external turbulent velocity is amplified to such a level that it is comparable with the velocity $\Gamma/2\pi\sigma$ in the vortex and therefore can significantly deform the vortex. It follows that $(\Gamma t_{ed}/2\pi\sigma^2)(\varepsilon^{1/3}\sigma^{1/3}) \approx \Gamma/2\pi\sigma$ implies that $t_{ed} \approx \sigma^{2/3}\varepsilon^{-1/3} \approx (\sigma/L)^{2/3}L/u_0$. Note that this deformation time is much less than the eddy time scale L/u_0 of the

https://doi.org/10.1017/S0022112099006990 Published online by Cambridge University Press

large-scale turbulence, but is independent of Γ provided that, initially, $\Gamma/2\pi\sigma$ is greater than u_0.

7. Summary

We have investigated, using linear theory (RDT), the distortion of the eddy structure and of the statistics of an external turbulent velocity field when it interacts with a columnar vortex. The turbulent eddies are stretched by the differential rotation to form structures like vortex rings (or spirals) wrapping around the columnar vortex, rapidly, within two or three revolutions. The statistical nature of the velocity field becomes axisymmetric, whereas that of the vorticity field remains asymmetric. The axial velocity component dominates near the vortex core surface and the radial velocity component dominates away from the core, which enhances the momentum and scalar transport in the radial direction. For small-scale turbulence, its energy decays radially like r^{-5}, grows in proportion to t^2, and increases with the length scale of the turbulence.

We have argued that nonlinear effects only change slightly the nature of these distorted flows, because the velocity field is approximately axisymmetric. However, initially the only significant pressure fluctuations on the main vortex are non-axisymmetric. Later the nonlinear effects reinforce the tendency of the vortices to become axisymmetric, and induce these induced vortices to move parallel to the columnar vortex. This leads to axisymmetric pressure fluctuations which can resonate with the natural waves of the columnar vortex. Time-dependent numerical experiments of Melander & Hussain (1993) and A. Wray (private communication) confirm the tendency of a strong vortex introduced into a turbulent flow to be bent by non-axisymmetric waves. Recent laboratory experiments (A. Srdic, private communication) on a fixed vortex produced by a rotating rod in grid turbulence show, by contrast, how a permanent undistorted vortex has sufficient time to distort the external turbulence into energetic random ring vortices. Their effect was apparent in the experiments by their movement along the columnar vortex and the energetic radial ejection of fluid from it.

T. M. is grateful to Japanese Ministry of Education for funding his visit to Cambridge. J. C. R. H. is grateful for useful conversations with Drs T. Poinsot and A. Corjon at CERFACS, Toulouse, to Dr A. Wray of Centre for turbulence research, and to Dr A. Srdic at Arizona State University, and for discussions with Professor F. Hussain at the University of Houston. We are also grateful to the referees for their suggestions.

Appendix A

In this Appendix, the actual forms of the velocity field calculated by RDT are given:

$$\tilde{M}_{11}(r,r';k_z,m) = \exp\left(-\frac{\mathrm{i}m\Gamma t}{2\pi r^2}\right)\left[\delta(r'-r) - \frac{K'_{|m|}(|k_z|r)}{K'_{|m|}(|k_z|r')}\delta(r'-\sigma)\right]$$
$$+|k_z|I'_{|m|}(|k_z|r)\frac{\mathrm{i}m\Gamma t}{\pi r'^2}\exp\left(-\frac{\mathrm{i}m\Gamma t}{2\pi r'^2}\right)K_{|m|}(|k_z|r')H(r'-r)$$

https://doi.org/10.1017/S0022112099006990 Published online by Cambridge University Press

$$-|k_z|K'_{|m|}(|k_z|r)\frac{I'_{|m|}(|k_z|\sigma)}{K'_{|m|}(|k_z|\sigma)}\frac{\mathrm{i}m\Gamma t}{\pi r'^2}\exp\left(-\frac{\mathrm{i}m\Gamma t}{2\pi r'^2}\right)K_{|m|}(|k_z|r')$$
$$+|k_z|K'_{|m|}(|k_z|r)\frac{\mathrm{i}m\Gamma t}{\pi r'^2}\exp\left(-\frac{\mathrm{i}m\Gamma t}{2\pi r'^2}\right)I_{|m|}(|k_z|r')H(r-r'), \tag{A 1a}$$

$$\tilde{M}_{12}(r,r';k_z,m) = -|k_z|I'_{|m|}(|k_z|r)\frac{|k_z|\Gamma t}{\pi r'}\exp\left(-\frac{\mathrm{i}m\Gamma t}{2\pi r'^2}\right)K'_{|m|}(|k_z|r')H(r'-r)$$
$$+|k_z|K'_{|m|}(|k_z|r)\frac{I'_{|m|}(|k_z|\sigma)}{K'_{|m|}(|k_z|\sigma)}\frac{|k_z|\Gamma t}{\pi r'}\exp\left(-\frac{\mathrm{i}m\Gamma t}{2\pi r'^2}\right)K'_{|m|}(|k_z|r')$$
$$-|k_z|K'_{|m|}(|k_z|r)\frac{|k_z|\Gamma t}{\pi r'}\exp\left(-\frac{\mathrm{i}m\Gamma t}{2\pi r'^2}\right)I'_{|m|}(|k_z|r')H(r-r'), \tag{A 1b}$$

$$\tilde{M}_{13}(r,r';k_z,m) = 0, \tag{A 1c}$$

$$\tilde{M}_{21}(r,r';k_z,m) = -\exp\left(-\frac{\mathrm{i}m\Gamma t}{2\pi r^2}\right)\frac{\mathrm{i}mK_{|m|}(|k_z|r)}{r|k_z|K'_{|m|}(|k_z|r')}\delta(r'-\sigma)$$
$$+\frac{\mathrm{i}m}{r}I_{|m|}(|k_z|r)\frac{\mathrm{i}m\Gamma t}{\pi r'^2}\exp\left(-\frac{\mathrm{i}m\Gamma t}{2\pi r'^2}\right)K_{|m|}(|k_z|r')H(r'-r)$$
$$-\frac{\mathrm{i}m}{r}K_{|m|}(|k_z|r)\frac{I'_{|m|}(|k_z|\sigma)}{K'_{|m|}(|k_z|\sigma)}\frac{\mathrm{i}m\Gamma t}{\pi r'^2}\exp\left(-\frac{\mathrm{i}m\Gamma t}{2\pi r'^2}\right)K_{|m|}(|k_z|r')$$
$$+\frac{\mathrm{i}m}{r}K_{|m|}(|k_z|r)\frac{\mathrm{i}m\Gamma t}{\pi r'^2}\exp\left(-\frac{\mathrm{i}m\Gamma t}{2\pi r'^2}\right)I_{|m|}(|k_z|r')H(r-r'), \tag{A 2a}$$

$$\tilde{M}_{22}(r,r';k_z,m) = \exp\left(-\frac{\mathrm{i}m\Gamma t}{2\pi r^2}\right)\delta(r'-r)$$
$$-\frac{\mathrm{i}m}{r}I_{|m|}(|k_z|r)\frac{|k_z|\Gamma t}{\pi r'}\exp\left(-\frac{\mathrm{i}m\Gamma t}{2\pi r'^2}\right)K'_{|m|}(|k_z|r')H(r'-r)$$
$$+\frac{\mathrm{i}m}{r}K_{|m|}(|k_z|r)\frac{I'_{|m|}(|k_z|\sigma)}{K'_{|m|}(|k_z|\sigma)}\frac{|k_z|\Gamma t}{\pi r'}\exp\left(-\frac{\mathrm{i}m\Gamma t}{2\pi r'^2}\right)K'_{|m|}(|k_z|r')$$
$$-\frac{\mathrm{i}m}{r}K_{|m|}(|k_z|r)\frac{|k_z|\Gamma t}{\pi r'}\exp\left(-\frac{\mathrm{i}m\Gamma t}{2\pi r'^2}\right)I'_{|m|}(|k_z|r')H(r-r'), \tag{A 2b}$$

$$\tilde{M}_{23}(r,r';k_z,m) = 0, \tag{A 2c}$$

$$\tilde{M}_{31}(r,r';K_z,m) = -\exp\left(-\frac{\mathrm{i}m\Gamma t}{2\pi r^2}\right)\frac{\mathrm{i}k_zK_{|m|}(|k_z|r)}{|k_z|K'_{|m|}(|k_z|r')}\delta(r'-\sigma)$$
$$+\mathrm{i}k_zI_{|m|}(|k_z|r)\frac{\mathrm{i}m\Gamma t}{\pi r'^2}\exp\left(-\frac{\mathrm{i}m\Gamma t}{2\pi r'^2}\right)K_{|m|}(|k_z|r')H(r'-r)$$

https://doi.org/10.1017/S0022112099006990 Published online by Cambridge University Press

$$-\mathrm{i}k_z K_{|m|}(|k_z|r)\frac{I'_{|m|}(|k_z|\sigma)}{K'_{|m|}(|k_z|\sigma)}\frac{\mathrm{i}m\Gamma t}{\pi r'^2}\exp\left(-\frac{\mathrm{i}m\Gamma t}{2\pi r'^2}\right)K_{|m|}(|k_z|r')$$
$$+\mathrm{i}k_z K_{|m|}(|k_z|r)\frac{\mathrm{i}m\Gamma t}{\pi r'^2}\exp\left(-\frac{\mathrm{i}m\Gamma t}{2\pi r'^2}\right)I_{|m|}(|k_z|r')H(r-r'), \tag{A 3a}$$

$$\tilde{M}_{32}(r,r';K_z,m) = -\mathrm{i}k_z I_{|m|}(|k_z|r)\frac{|k_z|\Gamma t}{\pi r'}\exp\left(-\frac{\mathrm{i}m\Gamma t}{2\pi r'^2}\right)K'_{|m|}(|k_z|r')H(r'-r)$$
$$+\mathrm{i}k_z K_{|m|}(|k_z|r)\frac{I'_{|m|}(|k_z|\sigma)}{K'_{|m|}(|k_z|\sigma)}\frac{|k_z|\Gamma t}{\pi r'}\exp\left(-\frac{\mathrm{i}m\Gamma t}{2\pi r'^2}\right)K'_{|m|}(|k_z|r')$$
$$-\mathrm{i}k_z K_{|m|}(|k_z|r)\frac{|k_z|\Gamma t}{\pi r'}\exp\left(-\frac{\mathrm{i}m\Gamma t}{2\pi r'^2}\right)I'_{|m|}(|k_z|r')H(r-r'), \tag{A 3b}$$

$$\tilde{M}_{33}(r,r';K_z,m) = \exp\left(-\frac{\mathrm{i}m\Gamma t}{2\pi r^2}\right)\delta(r'-r). \tag{A 3c}$$

REFERENCES

Basson, A. P. & Gilbert, A. D. 1998 The spiral wind-up of vorticity in an inviscid planar vortex. *J. Fluid Mech.* **371**, 109–140.

Batchelor, G. K. & Proudman, I. 1954 The effect of rapid distortion of a fluid in turbulent motion. *Q. J. Mech. Appl. Maths* **7**, 83–103.

Cambon, C. & Jacquin, L. 1989 Spectral approach to non-isotropic turbulence subjected to rotation. *J. Fluid Mech.* **202**, 295–318.

Cambon, C. & Scott 1999 Linear and nonlinear models of anisotropic turbulence. *Ann. Rev. Fluid Mech.* **31**, 1–53.

Carruthers, D. J. & Hunt, J. C. R. 1986 Velocity fluctuations near an interface between a turbulent region and a stably stratified layer. *J. Fluid Mech.* **165**, 475–501.

Ffowcs Williams, J. E. & O'Shea, S. 1970 Sound generation by hydrodynamic sources near a cavitated line vortex. *J. Fluid Mech.* **43**, 675–688.

Fukumoto, Y. & Miyazaki, T. 1996 Local stability of two-dimensional steady irrotational solenoidal flows with closed streamlines. *J. Phys. Soc. Japan* **65**, 107–113.

Gilbert, A. D. 1993 A cascade interpretation of Lundgren's stretched spiral vortex model for turbulent fine structure. *Phys. Fluids* A **5**, 2831–2834.

Goldstein, M. E. 1978 Unsteady vortical and entropic distortion of potential flow round arbitrary obstacles. *J. Fluid Mech.* **89**, 433–468.

Hunt, J. C. R. 1973 A theory of turbulent flow round two-dimensional bluff bodies. *J. Fluid Mech.* **61**, 625–706.

Hunt, J. C. R. 1984 Turbulence structure in thermal convection and shear-free boundary layers. *J. Fluid Mech.* **138**, 161–184.

Hunt, J. C. R. & Carruthers, D. J. 1990 Rapid distortion theory and the 'problems' of turbulence. *J. Fluid Mech.* **212**, 497–532.

Hunt, J. C. R. & Hussain, F. 1991 A note on velocity, vorticity and helicity of inviscid fluid elements. *J. Fluid Mech.* **229**, 569–587.

Hunt, J. C. R. & Graham, J. M. R. 1978 Free-stream turbulence near plane boundaries. *J. Fluid Mech.* **84**, 209–235.

Hussain, F. 1986 Coherent structures and turbulence. *J. Fluid Mech.* **173**, 303–356.

Keller, J. J. & Escudier, M. P. 1980 Theory and observations of waves on hollow-core vortices. *J. Fluid Mech.* **99**, 495–511.

Kelvin, Lord 1880 Vibrations of a columnar vortex. *Phil. Mag.* **10**, 155–168.

https://doi.org/10.1017/S0022112099006990 Published online by Cambridge University Press

Kevlahan, N. K.-R. & Hunt, J. C. R. 1997 Nonlinear interactions in turbulence with strong irrotational straining. *J. Fluid Mech.* **337**, 333–364.

Kida, S. & Tanaka, M. 1994 Dynamics of vortical structures in a homogeneous shear flow. *J. Fluid Mech.* **274**, 43–68.

Lee, M. J. & Hunt, J. C. R. 1989 The structure of shear turbulence near a plane boundary. In *Proc. Seventh Symp. on Turbulent Shear Flows*, *Stanford University*, pp. 8.1.1–8.1.6.

Lee, M. J., Kim, J. & Moin, P. 1987 Turbulent structure at high shear rate. In *Turbulent Shear Flows 6*, pp. 22.6.1–22.6.6. Springer.

Marshall, J. S. 1997 The flow induced by periodic vortex rings wrapped around a columner vortex core. *J. Fluid Mech.* **345**, 1–30.

Melander, M. V. & Hussain, F. 1993 Coupling between a coherent structure and fine-scale turbulence. *Phys. Rev.* E **48**, 2669–2689.

Risso, F., Corjon, A. & Stoessel, A. 1995 Direct numerical simulation of trailing vortices in homogeneous turbulence. *AIAA Paper* 96-0820.

Saffman, P. G. 1973 Structure of turbulent line vortices. *Phys. Fluids* **16**, 1182–1188.

Saffman, P. G. 1992 *Vortex Dynamics*, Chap. 11. Cambridge University Press.

Sarpkaya, T. & Suthon, P. 1991 Interaction of a vortex couple with a free surface. *Exps. Fluids* **11**, 205.

Spalart, P. R. & Wray, A. A. 1996 Initiation of the Crow instability by atmospheric turbulence. In *Proc. Symp. on The Characterisation and Modification of Wakes from Lifting Vehicles in Fluids.* AGARD-CP-584, pp. 18-1–18-8.

Sreedhar, M. K. & Ragab, S. A. 1994*a* Large eddy simulation of a longitudinal vortex. *AIAA Paper* 94-0529.

Sreedhar, M. K. & Ragab, S. A. 1994*b* Large eddy simulation of a longitudinal stationary vortices. *Phys. Fluids* **6**, 2501.

Townsend, A. A. 1976 *Structure of Turbulent Shear Flow*. Cambridge University Press.

Weber, W. 1868 Uber eine Transformation der hydrodynamischen Gleichungen. *J. Reine Angew. Math.* **68**, 286.

https://doi.org/10.1017/S0022112099006990 Published online by Cambridge University Press